CHARACTERISTICS OF ADAPTIVE BEAMFORMING METHODS IN AN HF BACKSCATTER ENVIRONMENT

Lloyd J. Griffiths

Colorado University

Prepared for:

Rome Air Development Center
Defense Advanced Research Projects Agency

August 1975

RADC-TR-75-205
Final Technical Report
August 1975

CHARACTERISTICS OF ADAPTIVE BEAMFORMING METHODS IN AN HF BACKSCATTER ENVIRONMENT

University of Colorado

Sponsored By
Defense Advanced Research Projects Agency
ARPA Order No. 1423

Approved for public release;
distribution unlimited.

The views and conclusions contained in this document are those of the authors and should not be interpreted as necessarily representing the official policies, either expressed or implied, of the Defense Advanced Research Projects Agency or the U. S. Government.

Rome Air Development Center
Air Force Systems Command
Griffiss Air Force Base, New York 13441

This report has been reviewed by the RADC Information Office (OI) and is releasable to the National Technical Information Service (NTIS). At NITS it will be releasable to the general public including foreign nations.

This report has been reviewed and is approved for publication.

APPROVED: Leonard Strauss

LEONARD STRAUSS
Project Engineer

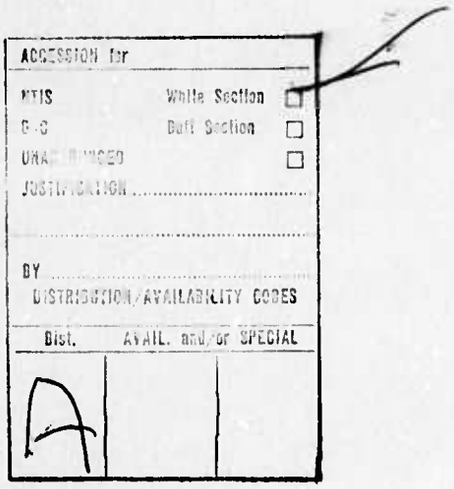

Do not return this copy. Retain or destroy.

UNCLASSIFIED

SECURITY CLASSIFICATION OF THIS PAGE *(When Data Entered)*

REPORT DOCUMENTATION PAGE		READ INSTRUCTIONS BEFORE COMPLETING FORM
1. REPORT NUMBER RADC-TR-75-205	2. GOVT ACCESSION NO.	3. RECIPIENT'S CATALOG NUMBER AD-A014354
4. TITLE *(and Subtitle)* CHARACTERISTICS OF ADAPTIVE BEAMFORMING METHODS IN AN HF BACKSCATTER ENVIRONMENT		5. TYPE OF REPORT & PERIOD COVERED Final Technical Report 1 Jan 72 - 31 May 75
		6. PERFORMING ORG. REPORT NUMBER N/A
7. AUTHOR(s) Lloyd J. Griffiths		8. CONTRACT OR GRANT NUMBER(s) F30602-72-C-0386
9. PERFORMING ORGANIZATION NAME AND ADDRESS University of Colorado Boulder CO 80302		10. PROGRAM ELEMENT, PROJECT, TASK AREA & WORK UNIT NUMBERS 62301E 14235101
11. CONTROLLING OFFICE NAME AND ADDRESS Defense Advanced Research Projects Agency 1400 Wilson Blvd Arlington VA 22209		12. REPORT DATE August 1975
		13. NUMBER OF PAGES 79
14. MONITORING AGENCY NAME & ADDRESS(if different from Controlling Office) Rome Air Development Center (OCSE) Griffiss AFB NY 13441		15. SECURITY CLASS. *(of this report)* UNCLASSIFIED
		15a. DECLASSIFICATION/DOWNGRADING SCHEDULE N/A

16. DISTRIBUTION STATEMENT *(of this Report)*

Approved for public release; distribution unlimited.

17. DISTRIBUTION STATEMENT *(of the abstract entered in Block 20, if different from Report)*

Same

18. SUPPLEMENTARY NOTES

RADC Project Engineer
Leonard Strauss (OCSE)

19. KEY WORDS *(Continue on reverse side if necessary and identify by block number)*

HF antenna arrays
Adaptive antenna arrays
Clutter filters
Time - dependent adaptive filters
Constrained adaptive filters
Aperture trade-off

20. ABSTRACT *(Continue on reverse side if necessary and identify by block number)*

The results summarized in this report were obtained during the period March 1, 1974 through March 31, 1975 and were carried out under RADC Contract No. F30602-72-C-0386 in support of the ARPA HF Adaptive Array Program. The objective of this program is to investigate the advantages which may accrue to HF backscatter systems employing adaptive beamforming methods. Data for the study were obtained using the Wide Aperture HF Radio Research Facility which is located in the central valley of California and operated by Stanford Research Institute,

DD FORM 1473 EDITION OF 1 NOV 65 IS OBSOLETE

UNCLASSIFIED

Menlo Park, California.

The efforts reported herein represent a continuation of previously reported studies and were directed toward obtaining detailed information regarding the performance of time-domain adaptive beamforming methods in an HF backscatter environment. It was shown that the time scale of coefficient variation in an adaptive processor operating in this environment is the order of one second. Successful tracking of the P-vector algorithm under these conditions was demonstrated. The use of MTI clutter suppression filters at the subarray outputs, prior to adaptation, was investigated. No significant improvement was observed with the use of these filters on experimental data.

A preliminary investigation into the effects of receive array aperture size on adaptive array performance has been carried out. It was shown that the presence of fading nulls can significantly effect the determination of optimal subarray location and spacing in an HF environment. In general, the adaptive beamformer performance was found to be less dependent upon array geometry than was the case for conventional processing.

A constrained minimum mean-square error time domain adaptive procedure suggested by Frost has been programmed and compared with the P-vector algorithm. Comparable performance was observed with a slight degradation in output SNR for the constrained case.

CHARACTERISTICS OF ADAPTIVE BEAMFORMING METHODS IN AN HF BACKSCATTER ENVIRONMENT

Lloyd J. Griffiths

Contractor: University of Colorado
Contract Number: F30602-72-C-0386
Effective Date of Contract: 1 January 1972
Contract Expiration Date: 31 March 1975
Amount of Contract: $62,508.00
Program Code Number: 4E20
Period of work covered: 1 January 1972 - 31 May 1975

Principal Investigator: Prof. Lloyd J. Griffiths
Phone: 303 492-7653

Project Engineer: Leonard Strauss
Phone: 315 330-3055

This research was supported by the Defense Advanced Research Projects Agency of the Department of Defense and was monitored by Leonard Strauss, RADC (OCSE), Griffiss AFB NY 13441.

CONTENTS

TABLES

ILLUSTRATIONS

I. SUMMARY

This report summarizes the technical results obtained under RADC Contract No. F 30602-72-C-0386 during the period March 1, 1974 through March 31, 1975. It is the final report on the University of Colorado's effort in support of the ARPA HF Adaptive Array Program. The work is a continuation of that reported earlier and has been carried out in close cooperation with the Remote Measurements Laboratory at Stanford Research Institute, Menlo Park, California. Data for the study were obtained using the WARF which is located in the central valley of California and which is operated by SRI.

Results have been obtained relating to the applicability of time-domain adaptation procedures in HF backscatter radar systems. Specifically, investigations regarding the performance of these procedures in an actual HF interference environment were conducted in four distinct areas:

1. Coefficient Time-Variation Studies:

It was shown that the time scale of coefficient variation in an HF environment was the order of about one second. These results indicate that block adaptation methods such as matrix inversion techniques must use an update interval of less than one-half second. It was further shown that the P-vector adaptation method can successfully track such variations in a 40 weight processor and that the standard

deviation of the resulting weights is accurately predicted by adaptive theory.

2. Clutter Suppression Studies

The use of individual three-pulse MTI clutter suppression filters at each subarray output has been investigated. For the experimental data studied, no significant advantage or disadvantage was observed with the use of these filters. Typical observed variations were the order of a few dB.

3. Aperture Tradeoff Studies

It was shown, using a simple simulation model and experimental data, that in a non-isotropic noise environment, conventional processing does not provide uniformly increasing performance with increased aperture size. It was further demonstrated that with adaptive processing, the improvement is a monotonically increasing function of aperture. The presence and effect of fading nulls on aperture utility was observed using experimental data. Such nulls can significantly affect the selection of optimal subarray location and spacing. Several examples demonstrating this phenomenon are presented.

4. Minimum Mean-Square Error Adaptation with Constraints

An alternative time-domain adaptation method, suggested by Frost, has been implemented and compared with the P-vector algorithm. Frost's procedure has the specific advantage of providing a flat frequency response in the main lobe

direction. It is demonstrated, however, that the extra degrees of freedom required to produce this response result in a lower output signal-to-total-noise ratio than that provided by P-vector adaptation. The amount of this degradation was observed to be as much as ten dB in some range-doppler cells.

Complete details of these results are presented in the sections following.

II. INTRODUCTION

This report is the final report on the University of Colorado's effort in support of the ARPA HF Adaptive Array Program. The results described herein represent a continuation of that described in References 1, 2, and 3. These references contain complete descriptions of the experimental equipment used for data collection as well as mathematical details regarding the structure of the P-vector adaptation algorithm used throughout this study.

The overall objective of the HF Adaptive Array Program has been to investigate the degree to which adaptive beamforming methods can improve the signal-to-noise ratio (SNR) observed at the output of an HF backscatter radar system. Efforts at the University of Colorado have been directed toward the development and analysis of specific adaptive algorithmic techniques designed to meet this objective. Data for the study were recorded using the Wide Aperture Research Facility (WARF) which is operated by the Stanford Research Institute, Menlo Park, California. Personnel at SRI have worked in close cooperation with the University of Colorado on this program and have developed and tested an on-line adaptive processing system for use at WARF. A recent SRI report[4] summarizes their effort.

The results summarized in the present report represent further investigations into the use of time-domain adaptation procedures in HF array applications and include the following

specific studies:

1. A study of the nature of the time-dependent behavior of adaptive weighting coefficients in the processor during adaptation on field recorded data.
2. An investigation into the use of clutter suppression filters (MTI filters) at the subarray receiver outputs and prior to adaptation.
3. An aperture study designed to measure performance versus receiving array aperture with an adaptive beamformer and to compare these results with those obtained using conventional beamforming methods.
4. A comparison of the P-vector adaptation algorithm with a constrained least-squares adaptive procedure suggested by Frost.[5]

Data for these studies were recorded using WARF during the months of March and November, 1974. Observations with the full WARF aperture were taken and included digitized recordings from eight subarray outputs with each subarray consisting of a filled 32 element linear array. Both eastward and westward looking tests were included in the data. Computer processing of these data was carried out using the CDC 6400 computing facility at the University of Colorado as well as several smaller computers within the Electrical Engineering Department at Colorado.

The experimental WARF configuration used to collect the data was identical with that reported previously[2,3]. A sawtooth sweep-frequency continuous-wave transmit signal similar

to that shown in Fig. 1 was employed for all tests. The characteristics of this waveform have been reported previously[3,4]. Briefly, at each receiving subarray, the signal was deramped using a local oscillator signal similar to that shown in Fig. 1 with a reset time delayed with respect to the transmitted waveform. The delay was chosen such that signals from the desired range fell within the 780 Hz receiver bandwidth while those from other ranges were rejected.

An analog-to-digital converter operating at a sampling rate of 1.920 kHz (32 samples per sweep) was used to digitize the deramped signals after they had been converted to baseband frequencies. Digitizing proceeded continuously in time with all samples being recorded on magnetic tape without interruption. A multiplexed sample and hold system provided simultaneous sampling of the eight subarray received outputs. Thus, the net digitizing rate was 8X1920=15.36 kHz. for the entire system.

Beamformed sampled output signals were generated at a later time from these recordings using the structure shown in Fig. 2. If $x_i(k)$ is the k^{th} sample from the i^{th} subarray, the beamformed output signal $y(k)$ is given by

$$y(k) = \sum_{i=1}^{8} \sum_{j=0}^{4} W_{ij}(k) x_i(k-j), \qquad (1)$$

where $W_{ij}(k)$ is the weighting coefficient at the i^{th} subarray which multiplies the signal after j units of delay. In general, these coefficients are time varying and determined by an adaptive algorithm. Thus, $W_{ij}(k)$ represents the coefficient after k samples of data have been received from each subarray and a

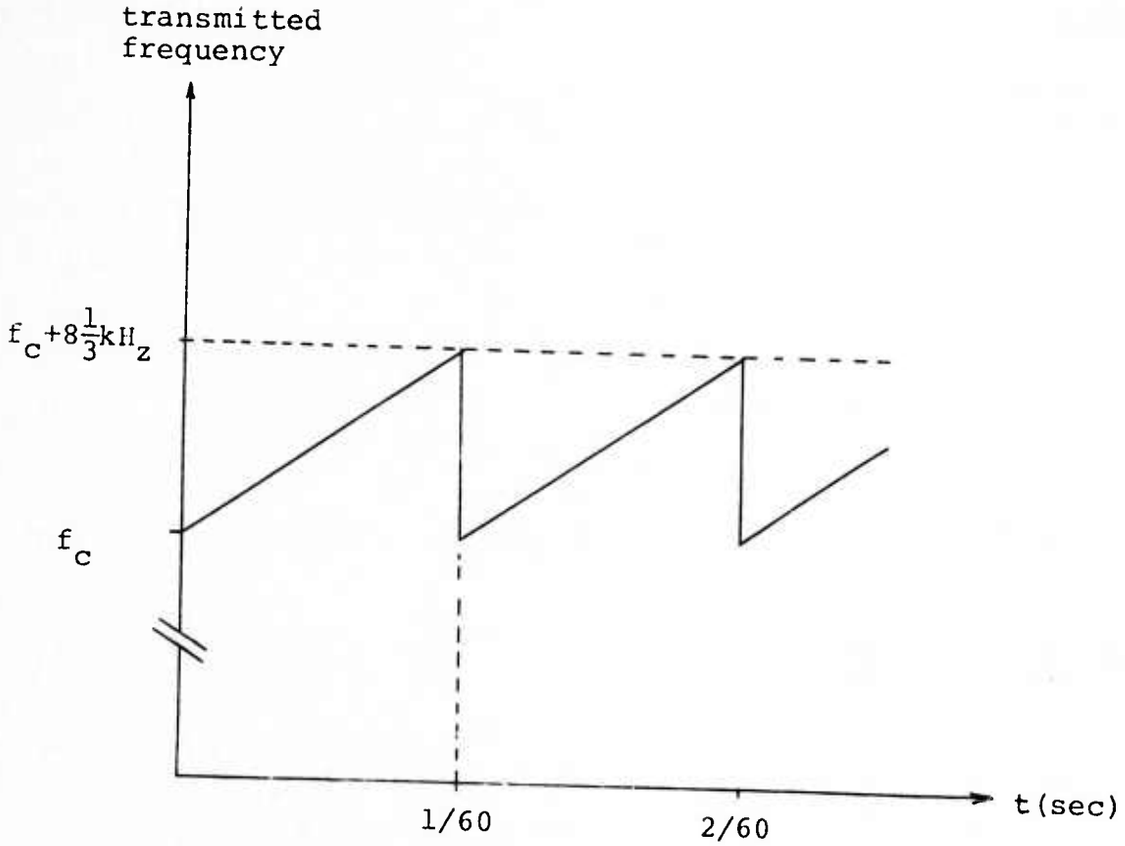

Fig. 1. Instantaneous frequency of transmitted waveform used during experimental tests

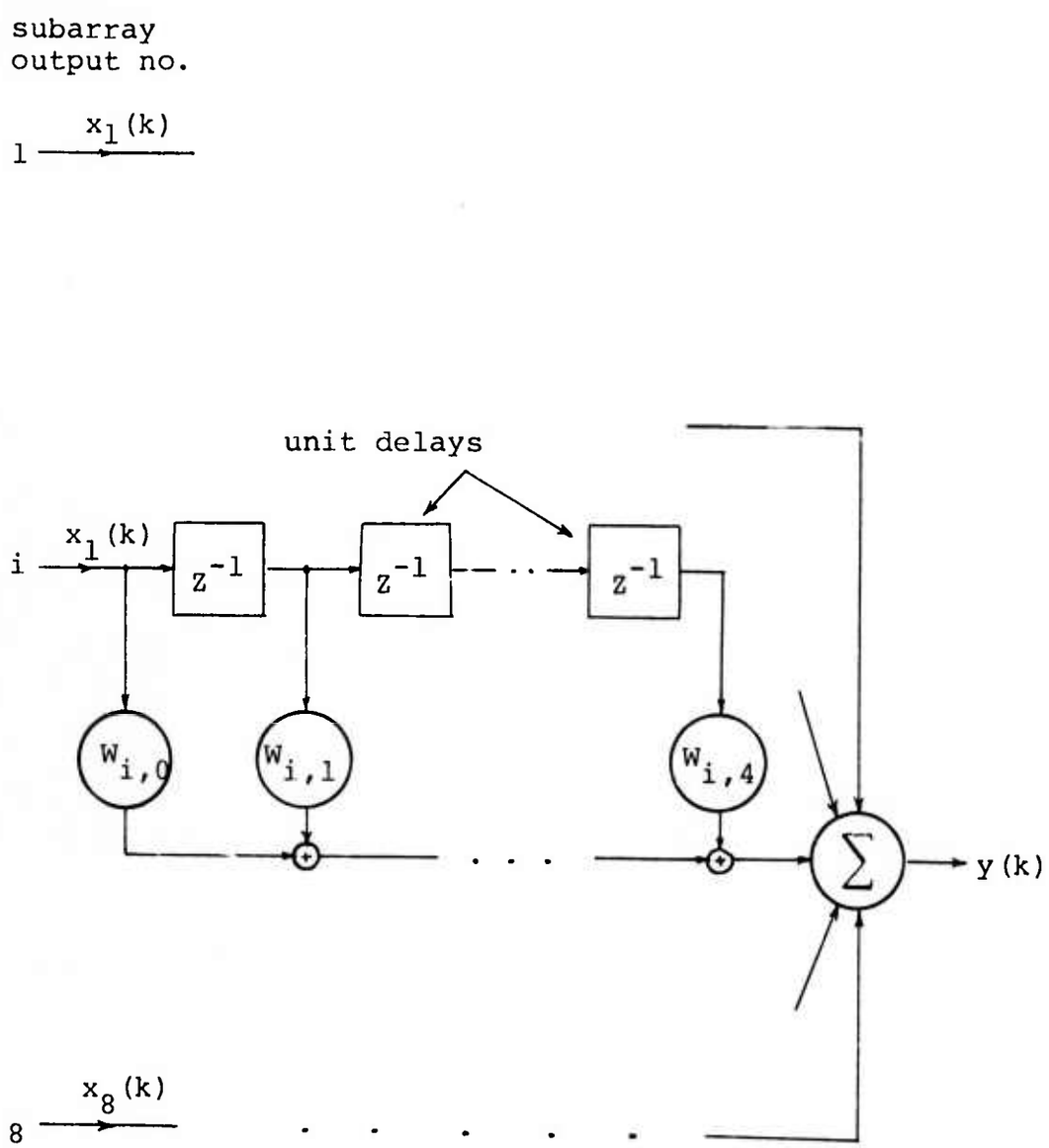

Fig. 2. Tapped-delay line array processing configuration used during experimental tests

corresponding k adaptations of each coefficient have taken place. Adaptations normally are carried out prior to the output computation given in (1). For example, in the case of the P-vector algorithm, the adaptation procedure is

$$W_{ij}(k+1) = W_{ij}(k)+u[p_{ij}-y(k)]x_i(k-j) \qquad (2)$$

where p_{ij} is the steering vector coefficient. A complete description of this algorithm and its convergence properties are presented in Reference 3.

As shown in Figure 2 and Eq. (1), a total of five coefficients per subarray were used in the processor. This number was held constant throughout the results presented herein, and was selected on the basis of the recommendations presented in a previous study[3].

Performance evaluation of adaptive beamformer performance was conducted on the basis of range-doppler processing of the output signal y(k). As previously discussed[3], a two-dimensional digital Fourier transform of 64 successive output sweeps (2048 samples total) results in a display with 16 resolvable range cells and 64 doppler cells. The resulting display represents range-doppler information taken over the past one second of real time. Figure 3 shows a typical range-doppler map derived in this manner. The plot has been normalized to provide an average noise floor level which is 15 db below the dynamic range of the display. Signals which exceed this range, such as the strong clutter returns discernible at zero doppler and all ranges, are clipped at the maximum plot value. The data for Fig. 3 were

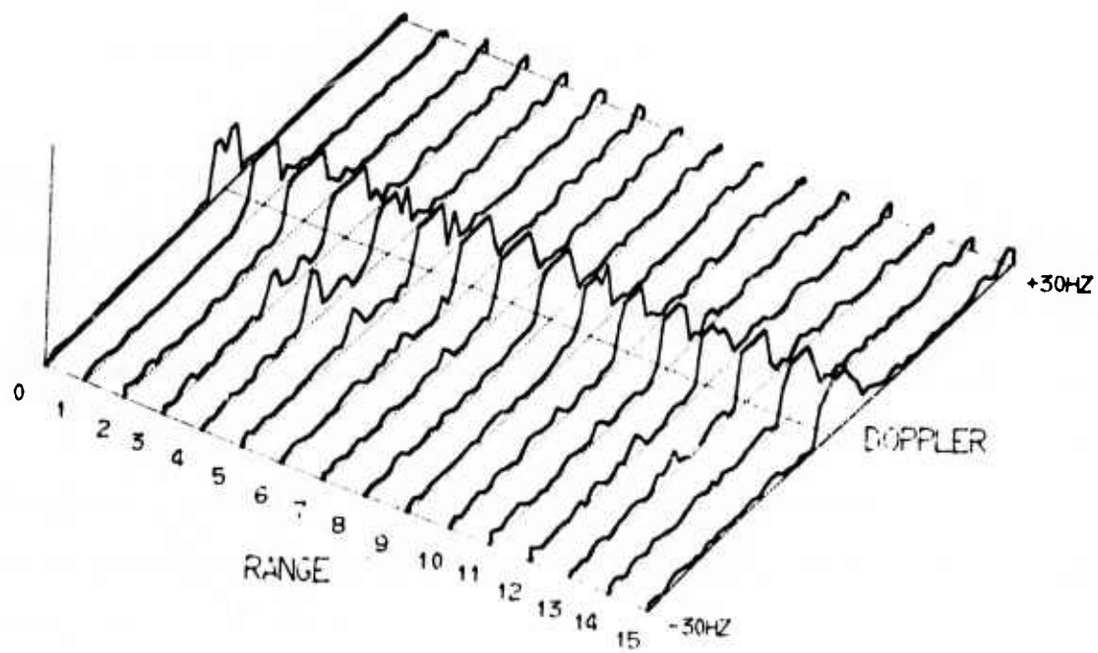

Fig. 3. Range-doppler map generated using one second average and coventional processing with eastward transmissions at 15.37 MHz on Nov. 8, 1974

taken on November 8, 1974 using eastward transmissions at 15.37 MHz. A strong target having a negative doppler frequency of about -10Hz can be seen centered in range cell four. A conventional beamforming system was used to generate this result. Conventional processing consists of using fixed weighting coefficients in the structure shown in Fig. 2 with the following Dolph taper[4] coefficients:

$$W_{1,0} = W_{8,0} = 0.355$$
$$W_{2,0} = W_{7,0} = 0.562$$
$$W_{3,0} = W_{6,0} = 0.841$$
$$W_{4,0} = W_{5,0} = 1.000$$
$$W_{i,j} = 0 \text{ all } i,\ j > 0.$$

Plots of this type were computed for both conventional and adaptive beamforming processors under a variety of signal, noise and interference conditions and are summarized in the sections following.

III. COEFFICIENT TIME-VARIATION STUDIES

The adaptive procedures of interest in this study are termed "time-domain" methods to indicate that the beamforming coefficients in the processor are changed as each new data sample is received. This is in contrast with matrix-inversion adaptive methods which are termed "block-average" techniques. In these latter methods, correlation properties of the received data are obtained through time averages which are generally taken over one dwell--i.e., over one second for the plot shown in Fig. 3. The resulting averages are used to construct a data autocorrelation matrix R_{XX} which is then inverted and multiplied by the steering vector P_{Xd} to generate a set of optimal coefficients W* (see Eq. (15) in [3]).

$$W^* = R_{XX}^{-1} P_{Xd} \tag{3}$$

This set of coefficients is used to combine the subarray signals observed over the dwell of interest. Thus, the output y(k) in Fig. 2 for the 2048 samples of the dwell is computed as

$$y(k) = \sum_{i=1}^{8} \sum_{j=0}^{4} w_{ij}^* x_i(k-j) \tag{4}$$

where the w_{ij}^* are determined by (3). The procedure is then repeated at the next dwell with a new set of correlations R_{XX} and resulting weights W*. The procedure is adaptive in the sense that a different set of weights is used to process each

dwell and the iteration interval of adaptation is equal to one dwell (2048 samples).

This is in marked contrast to the P-vector algorithm method of adaptation. In matrix form (see Eq. (19) in [3]), the algorithm (2) is given by

$$W(k+1) = W(k)+u[P_{Xd}-y(k)]X(k) \tag{5}$$

where

$$W(k) = \begin{bmatrix} W_{1,0}(k) \\ W_{2,0}(k) \\ \vdots \\ W_{8,0}(k) \\ W_{1,1}(k) \\ \vdots \\ W_{8,4}(k) \end{bmatrix} \tag{6}$$

$$X(k) = \begin{bmatrix} x_1(k) \\ x_2(k) \\ \vdots \\ x_8(k) \\ x_1(k-1) \\ \vdots \\ x_8(k-4) \end{bmatrix} \tag{7}$$

It can be shown that[3] under conditions of a stationary environment, the P-vector algorithm (5) and the matrix inversion method will produce, on the average, identical coefficient vectors, i.e.

$$\lim_{k\to\infty} E[W(k)] = RHS[W^*] \qquad (8)$$

where $E[\cdot]$ denotes expectation.

The primary advantage of adaptive array processing methods in HF applications is their capability to adapt to time-variations in HF signals which are caused by ionospheric fluctuations. In effect, the processors act as time-varying linear filters and provide interference immunity by continually changing the array pattern so as to minimize the effects of noise and interference at the beamformed output. The effectiveness of an adaptive beamformer in providing null tracking is clearly dependent upon the time scale of the ionospheric changes with respect to the adaptation update interval.

Figures 4 through 8 show the range-doppler maps which were computed for data collected on March 15, 1974. The transmitted signals for these data were directed eastward at a center frequency of 12.37 MHz. Plots for both conventional and P-vector processing are presented. A proportionality constant of $\alpha = 0.1$ (see Eq. (27), Ref. 3) was used for these examples. The target of interest is visible on range cells 6 and 7 at a doppler frequency of about -15 Hz. The strong bands of energy observed at -21, -9, +7, and +23 Hz doppler frequencies are interference lines. This test was intentionally conducted under conditions of strong HF interference to illustrate the capabilities of the adaptive processor and the advantages are readily apparent in these figures.

Coefficient time-variation studies were carried out for the adaptive coefficients used to generate the plots shown in

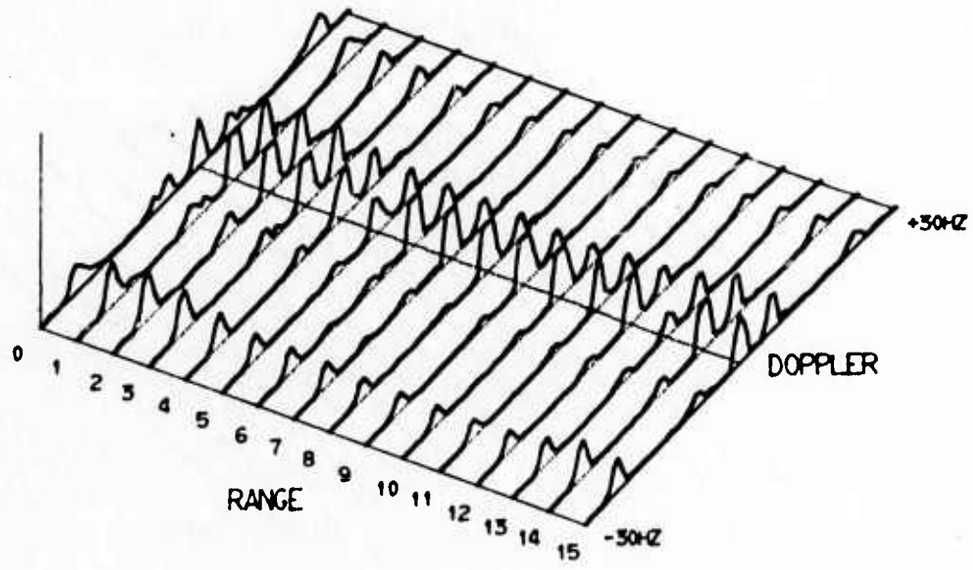

a) Conventional processing

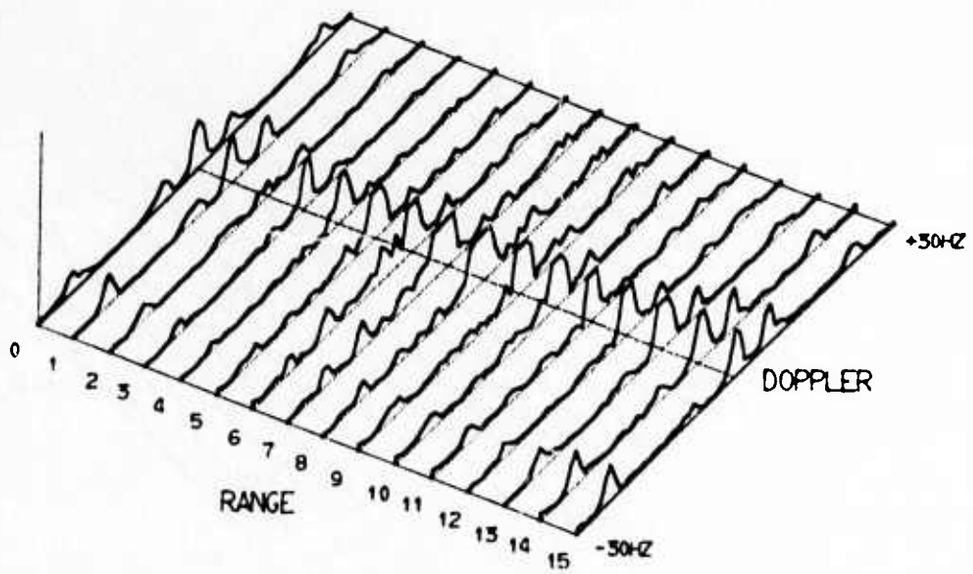

b) P-vector adaptive processing, α=0.1

Fig. 4. Range-doppler map for dwell no. 1, March 15, 1974

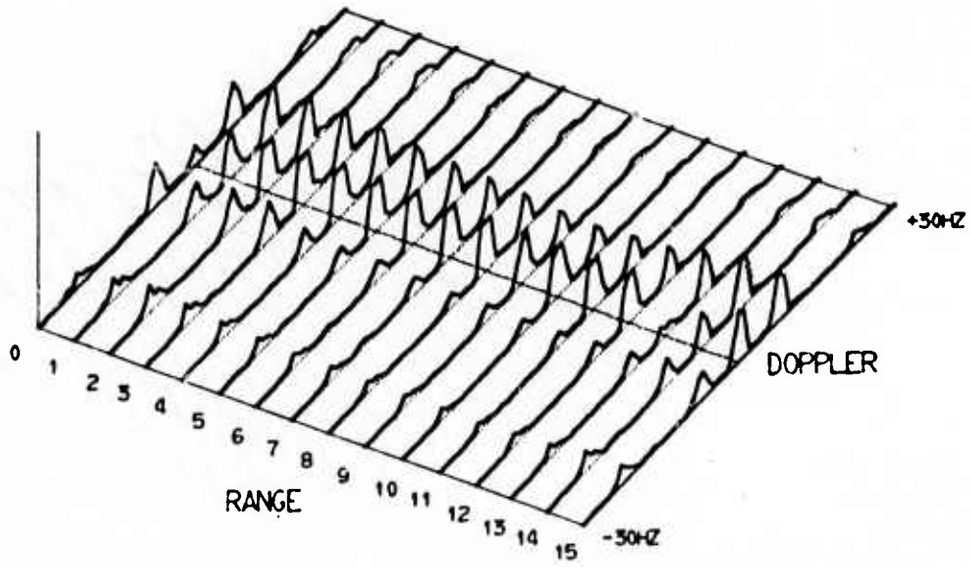

a) Conventional processing

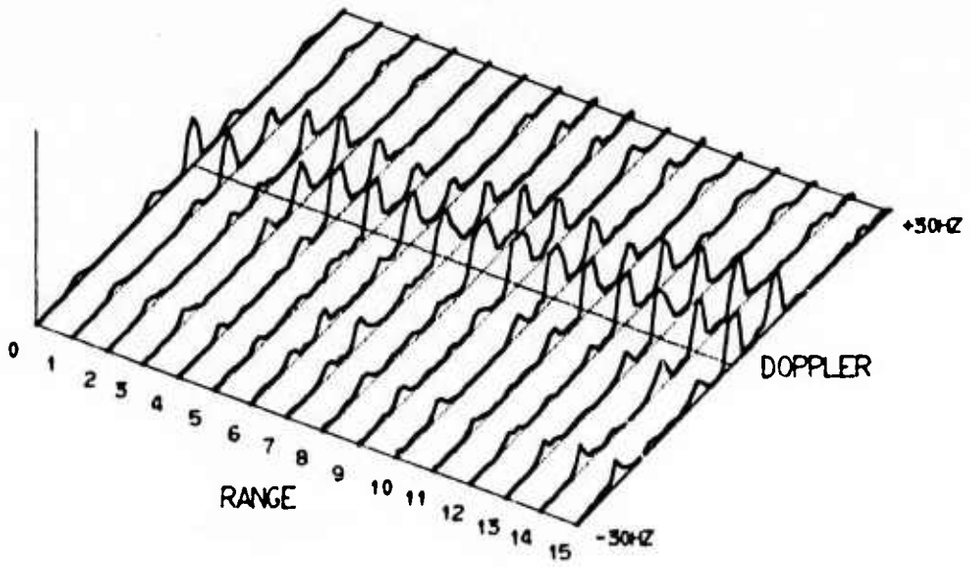

b) P-vector adaptive processing, $\alpha=0.1$

Fig. 5. Range-doppler map for dwell no. 2, March 15, 1974

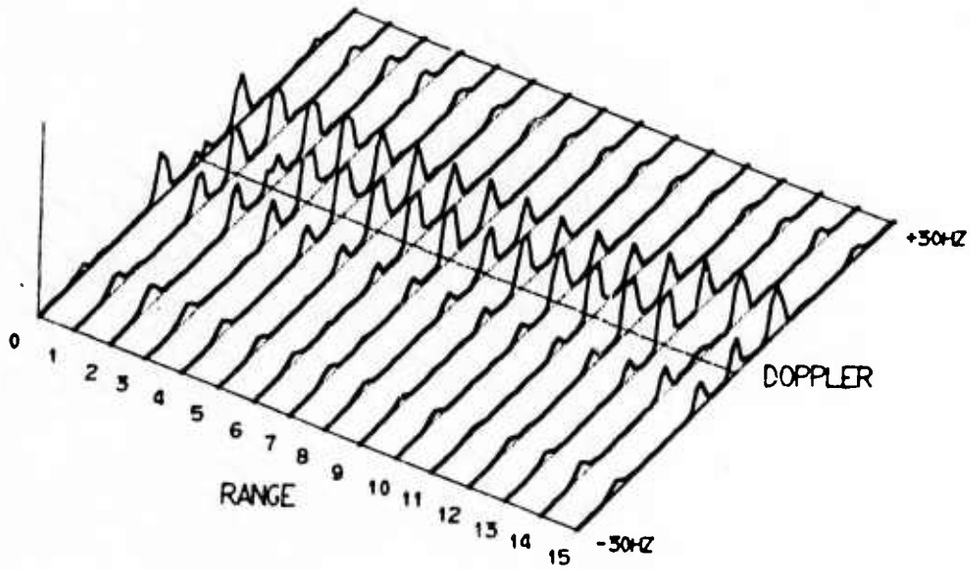

a) Conventional processing

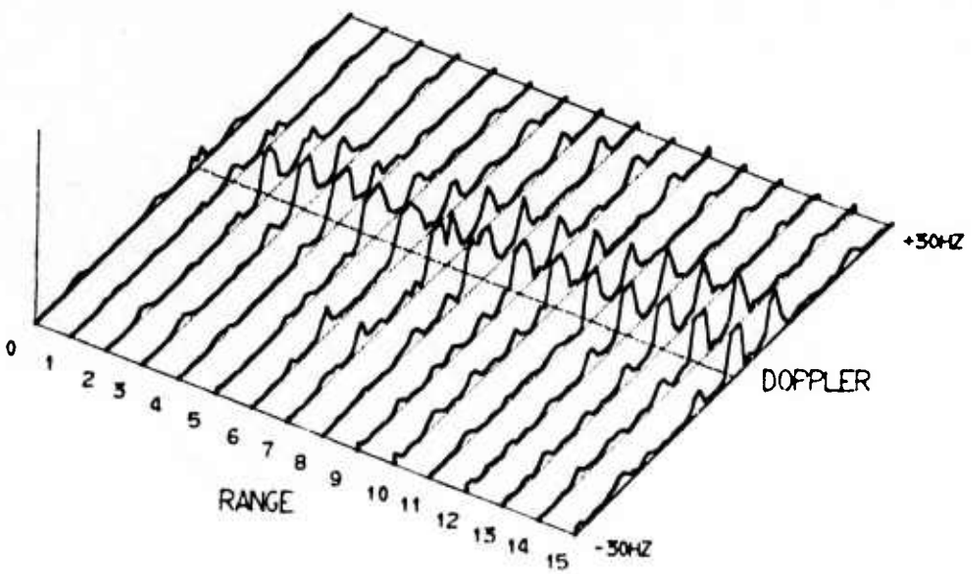

b) P-vector adaptive processing, α=0.1

Fig. 6. Range-doppler map for dwell no. 3, March 15, 1974

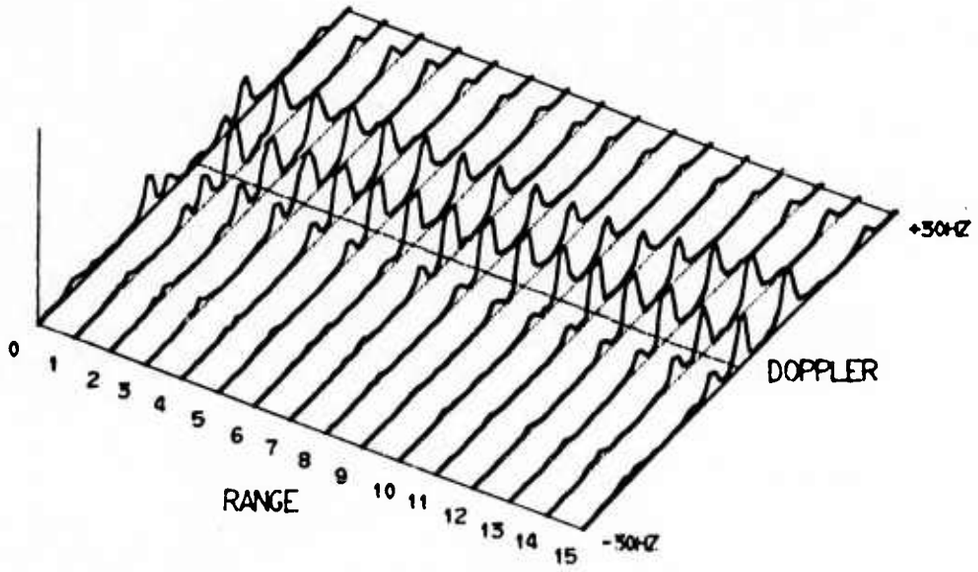

a) Conventional processing

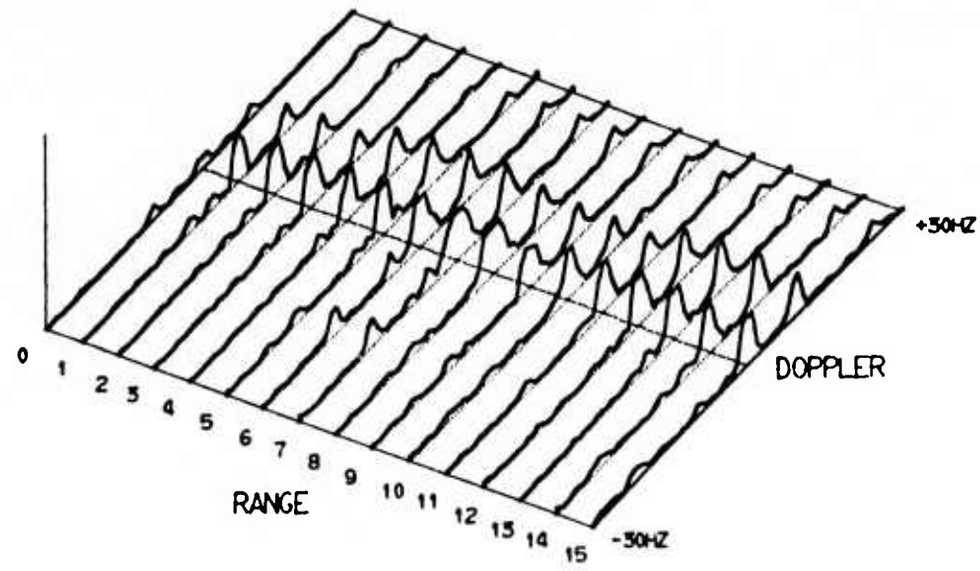

b) P-vector adaptive processing, $\alpha=0.1$

Fig. 7. Range-doppler map for dwell no. 4, March 15, 1974

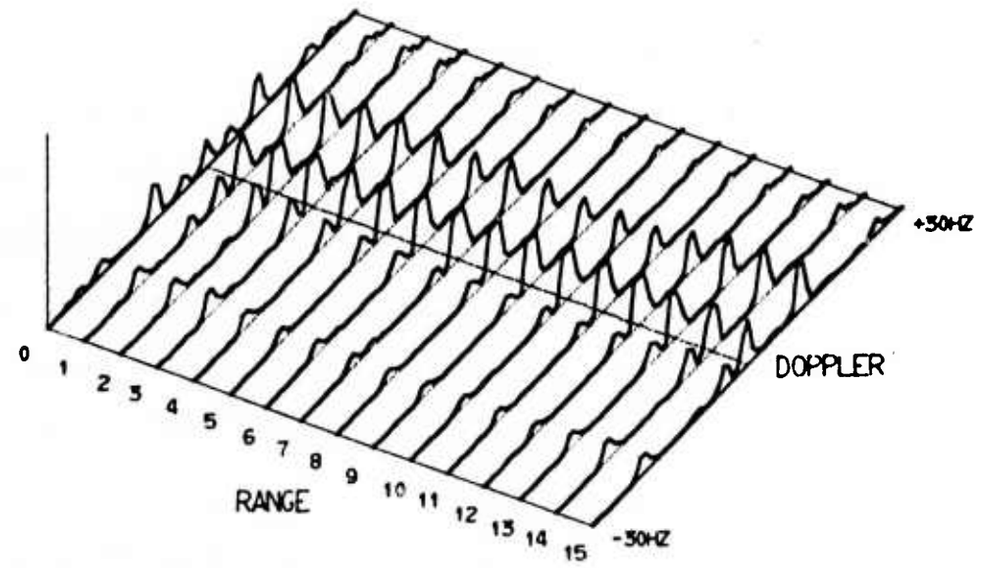

a) Conventional processing

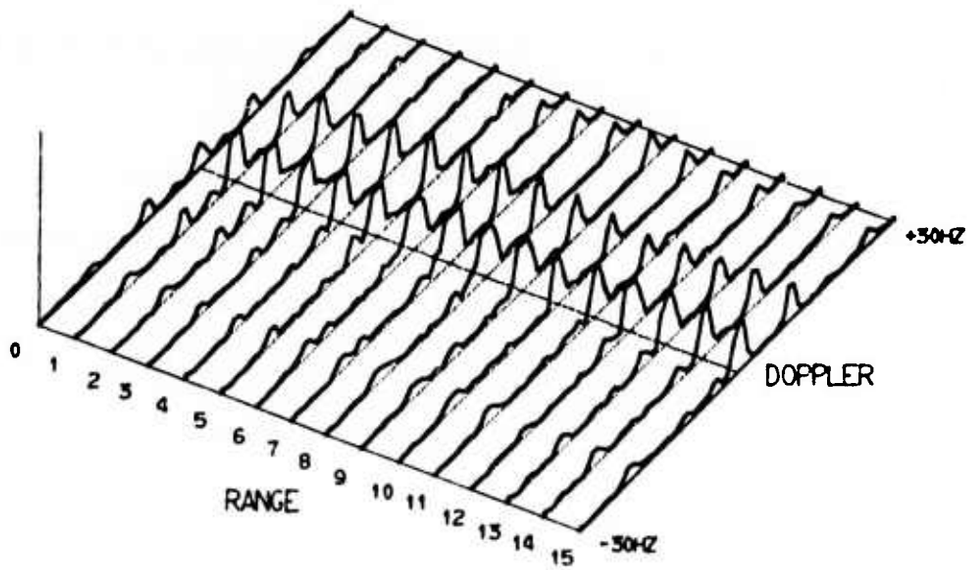

b) P-vector adaptive processing, $\alpha=0.1$

Fig. 8. Range-doppler map for dwell no. 5, March 15, 1974

Figs. 4b) to 8b). As the processor adapted on these data, the mean and standard deviation of each coefficient in the filter was computed at intervals of 128 samples or 4 sweeps. Since each dwell represents an average over 64 successive sweeps, a total of 16 mean and standard deviation values were computed for each coefficient per dwell. The results of this calculation are presented in Figs. 9 and 10. Figure 9 presents the values observed for the five coefficients used to process the output of subarray #1 and Fig. 10 illustrates the values observed at the first coefficient or elements #1 through #5. Standard deviation bars are shown less frequently than the mean values for purposes of clarity. Although graphs are presented for only 9 of the 40 weights in the processor, similar curves were observed for other coefficients as well as for other experimental test configurations.

Computations were also carried out to determine the average behavior of the coefficient values over one complete dwell. Table I summarizes representative results obtained in this manner. In each case, the mean and standard deviations were carried out using the following averaging procedure:

$$\bar{M}_{ij} = \frac{1}{16} \sum_{m=1}^{16} M_{ij}(m) \tag{9}$$

$$\bar{\sigma}_{ij} = \frac{1}{16} \sum_{m=1}^{16} \sigma_{ij}(m) \tag{10}$$

where $M_{ij}(m)$ and $\sigma_{ij}(m)$ are the coefficient 128 point sample mean and standard deviations within the dwell of interest, as shown in Figs. 9 and 10. For example, with m=1 and using the first dwell,

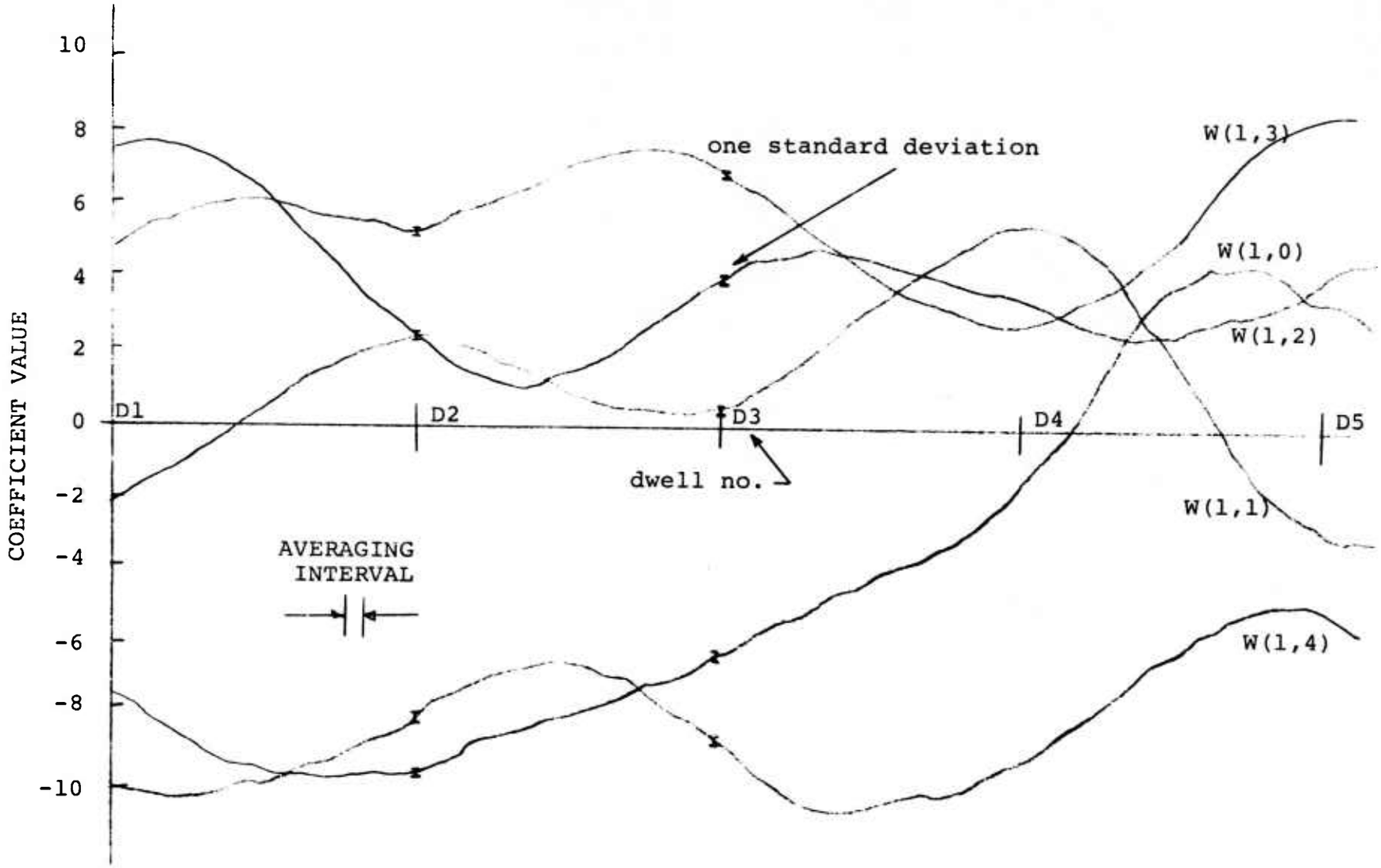

Fig. 9. Time history of coefficient values for data shown in Figs. 4-8, first 5 coefficients on subarray no. 1

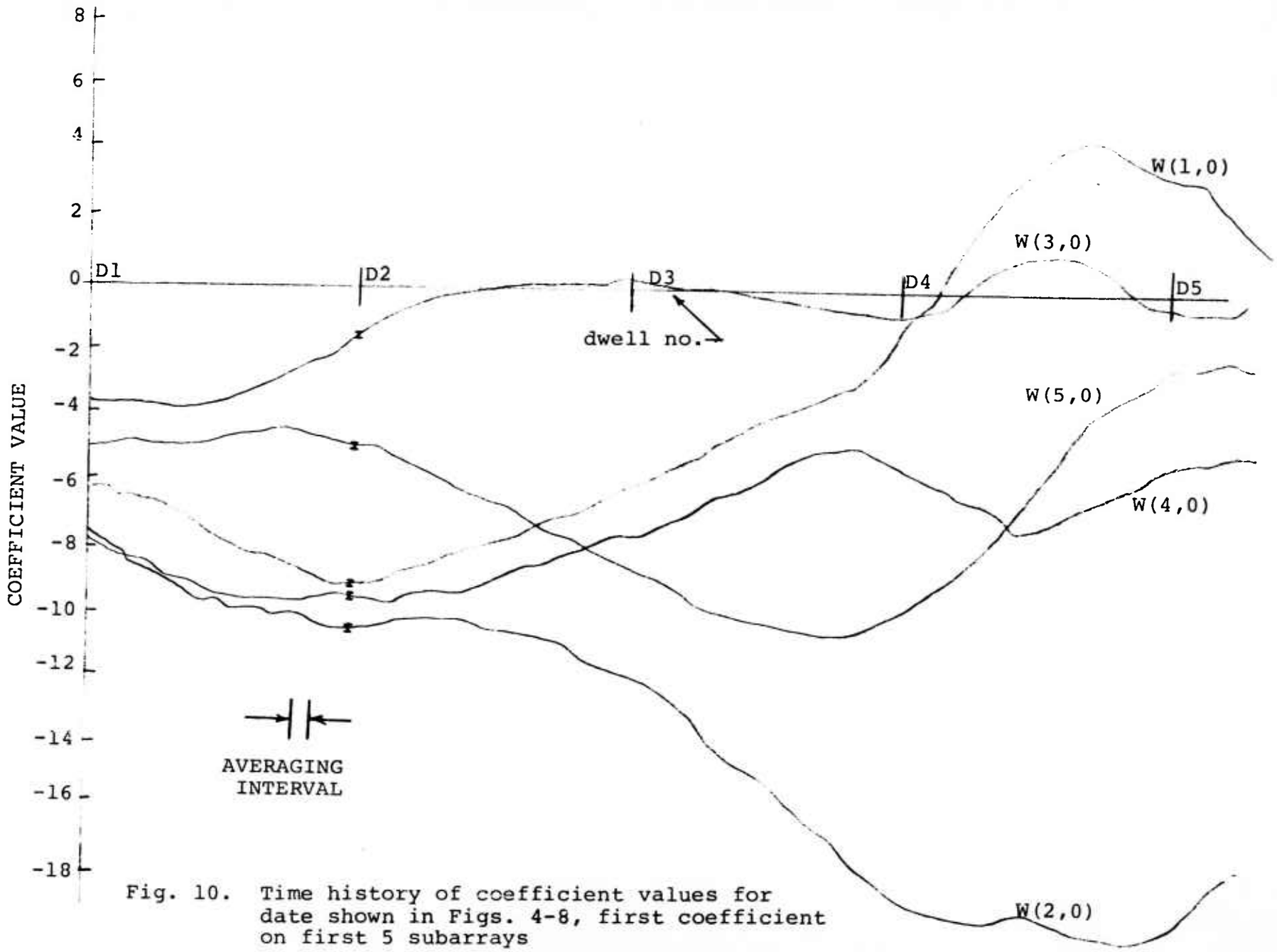

Fig. 10. Time history of coefficient values for date shown in Figs. 4-8, first coefficient on first 5 subarrays

Table I

Mean and Standard Deviation Coefficient Values

Averaged Over One Dwell

coefficient	dwell no.	mean	std dev	% dev
W_{10}	1	-9.24	.069	.75
	2	-8.04	.093	1.15
	3	-4.25	.093	2.19
	4	2.32	.165	7.10
W_{12}	1	6.16	.078	1.27
	2	1.87	.106	5.63
	3	4.34	.066	1.53
	4	2.92	.104	3.57
W_{14}	1	-9.65	.066	.68
	2	-7.10	.069	.97
	3	-9.88	.097	.98
	4	-6.85	.089	1.31
W_{50}	1	-4.88	.074	1.52
	2	-6.65	.108	1.62
	3	-10.04	.093	.93
	4	-7.13	.173	2.42

$$M_{ij}(1) = \frac{1}{128} \sum_{k=1}^{128} W_{ij}(k) \tag{11}$$

$$\sigma_{ij}(1) = \sqrt{\frac{1}{128} \sum_{k=1}^{128} [W_{ij}(k) - M_{ij}(1)]^2} \tag{12}$$

It should be noted that $\bar{\sigma}_{ij}$ in (10) is not equal to the standard deviation of the coefficient over one complete dwell. This particular method of averaging is used here to eliminate variations caused by the time varying means shown in Figs. 9 and 10.

An "average coefficient variation" γ similar to that defined in Equation (35) of Reference 3 was computed for the four dwells shown in Figs. 9 and 10. The results, expressed as a percentage, are given in Table II.

Table II

Average Coefficient Variation γ

Dwell No.	γ
1	1.06
2	2.34
3	1.41
4	3.54

Several observations are apparent from these results. The large scale mean weight variations shown in Figs. 9 and 10 can only be attributed to statistical changes in the received data. Variations caused by use of the time domain P-vector algorithm produce measured fluctuations which are the order of a few percent. These values are consistent with theoretical values previously published for this algorithm[3] under conditions of

stationary input statistics and an α value of 0.1. In effect, the time variation of the input statistics is sufficiently slow that adaptive tracking is excellent. The agreement between the γ values in Table II above and that published in Ref. 3 is further evidence of this fact. Inspection of Figs. 9 and 10 also reveals that while the input time variation is slow with respect to the adaptive time constant, it is of the same time scale as the dwell interval. Several cases of marked variations within one second are apparent in these results. For the case of a two second dwell, such has been proposed for HF backscatter radar applications, this variation would be even more noticeable. Further discussion and conclusions based on these observations are presented in Section VII below.

IV. CLUTTER SUPPRESSION STUDIES

In an HF backscatter radar system, signals returned from stationary targets such as ground backscatter appear in the processed range-doppler map as being spread over all range bins and centered at 0 Hz doppler with a doppler spread of about 1 Hz due to ionospheric variations. Figs. 4 through 8 show several examples of ground-backscatter returns, generally termed clutter returns. One common method of removing these signals from the display is through the use of a moving target indication (MTI) filter at the beamformer output. The general approach in the use of such filters is to combine signals from J adjacent sweeps using coefficients c_ℓ. Thus, if $y_j(k)$ is the k^{th} time sample of the beamformed output during the j^{th} sweep, with index k having a zero value at the start of each sweep, an MTI output signal $z_j(k)$ for sweep j is formed as

$$z_j(k) = \sum_{\ell=0}^{J-1} c_\ell y_{j-\ell}(k) \qquad (13)$$

The simplest case occurs when c_0=+ 1/2 and c_1=- 1/2, the two-pulse MTI filter, and adjacent sweeps are subtracted. Stationary targets are eliminated due to the fact that they have the same received waveform in each sweep. More complex filtering operations are best described in terms of the effect of the operation in Eq.(13) on the resulting range-doppler display. Since the c_ℓ coefficients are not functions of k, they must have a constant effect in the range domain. Inspection of (13),

however, indicates that these coefficients perform a convolution filtering operation across the sweeps, for each specific value of k. Since doppler information is obtained by a Fourier Transform across the sweeps, the effect of this filter in the doppler domain is to multiply the doppler spectrum by a function $c(\omega_d)$ given by

$$c(\omega_d) = \sum_{\ell=0}^{J-1} c_\ell e^{-j2\pi\omega_d \ell/\omega_0} \tag{14}$$

where ω_d is the doppler frequency of interest and ω_0 is determined by the sweep repetition rate. For the 60 Hz repetition used in the present study, $\omega_0 = 2\pi \times 60$ radians/sec. In summary, the effect of the MTI operation defined in (13) is to multiply the doppler spectrum for each range bin by the filtering function defined in Eq. (14).

Thus, for the two-pulse MTI filter, the doppler filter is

$$c(\omega_d) = \tfrac{1}{2} - \tfrac{1}{2}e^{-j2\pi\omega_d/\omega_0} \tag{15}$$

$$|c(\omega_d)| = |\sin \pi\omega_d/\omega_0| \tag{16}$$

The magnitude function for this filter is shown in Fig. 11. Note that signals received at zero doppler are perfectly attenuated $|c(0)| = 0$ while those received at the doppler fold over frequencies $\pm\omega_{0/2}$ are unaffected by the MTI operation $|c(\pm\omega_0/2)| = 1$.

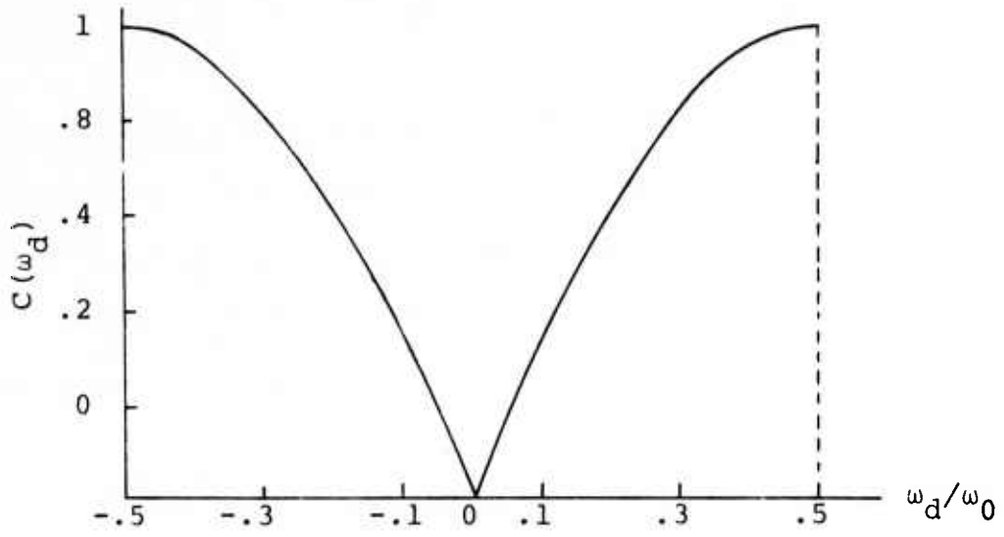

Fig. 11. Doppler spectrum equivalent filter for two-pulse MTI clutter suppression

The problem of designing clutter rejection filters with a desired magnitude function $c(\omega_d)$ is a classical problem in digital filter design and many references on the subject are available.[6,7] In general, larger values of J provide greater flexibility in this design but also impose a longer build-up time in the filter. For example, a 32 pulse MTI filter would require 32 sweeps or about 1/2 second to achieve cancellation.

The MTI filters used in the present study were three pulse with coefficients given by

$$C_0 = 1/4$$
$$C_1 = -1/2$$
$$C_2 = 1/4$$

The equivalent doppler function is then

$$c(\omega_d) = \tfrac{1}{2} - \tfrac{1}{4}e^{-j2\pi\omega_d/\omega_0} + \tfrac{1}{2}e^{-j4\pi\omega_d/\omega_0} \qquad (17)$$

$$|c(\omega_d)| = |\sin^2 \pi \omega_d/\omega_0| \qquad (18)$$

and is plotted in Fig. 12.

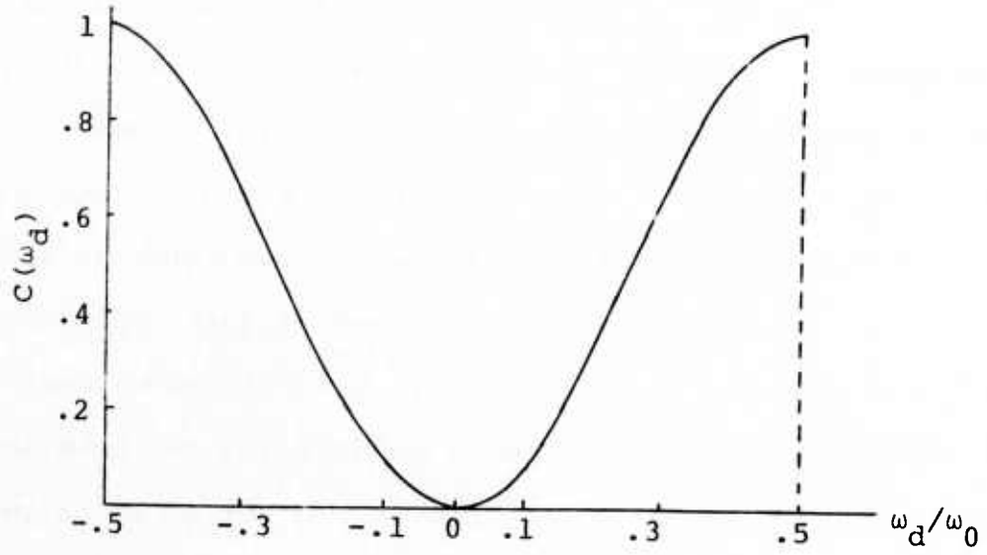

Fig. 12. Doppler spectrum equivalent filter for three-pulse MTI clutter suppression

Clutter Suppression in Adaptive Beamforming

The primary advantage of MTI clutter suppression in conventional radar systems is the available increase in dynamic range. Removal of the clutter energy prior to analog-to-digital conversion allows more efficient use of the digitizer in that the gain level is controlled by desired signals and/or interference, which may be 40 db below the clutter. Thus, a larger number of bits can be devoted to conversion of the signal and interference components than is the case when the gain level is controlled by the clutter energy.

In the case of adaptive beamforming, there is an additional possible advantage of MTI processing. Figure 13 shows a proposed configuration for clutter suppression in an adaptive beamformer. Note that because the MTI filters are placed after A/D conversion, no advantage in dynamic range can be achieved A digital three-pulse MTI processor was placed at the sampled output of each of the eight subarrays. Thus, the signal which reached the adaptive tapped-delay line filter attached to each subarray had little clutter energy present. The advantage of this implementation is that the adaptive degrees of freedom in the beamformer can be applied directly to interference suppression and need not be taken up with the elimination of clutter. A series of calculations were carried out to test this hypothesis. The data used were those shown in Figs. 4-8. Identical data for each dwell were processed with and without the MTI filters. In both cases, P-vector adaptation was employed with $\alpha = 0.1$. The range-doppler comparisons for the five dwells of interest are presented in Figs. 14-18.

In order to better analyze the behavior of these MTI filters, signal to noise ratio and signal to interference plots were derived from these data. The measurements were carried out, respectively, by plotting received amplitude level as a function of range, with doppler fixed at the target doppler and secondly as a function of doppler with range fixed at the target range. Two such plots, computed for dwell no. 3, are shown in Figs. 19 and 20. In effect, the plots represent two perpendicular cross-sections taken through the range doppler map presented in Fig. 16,

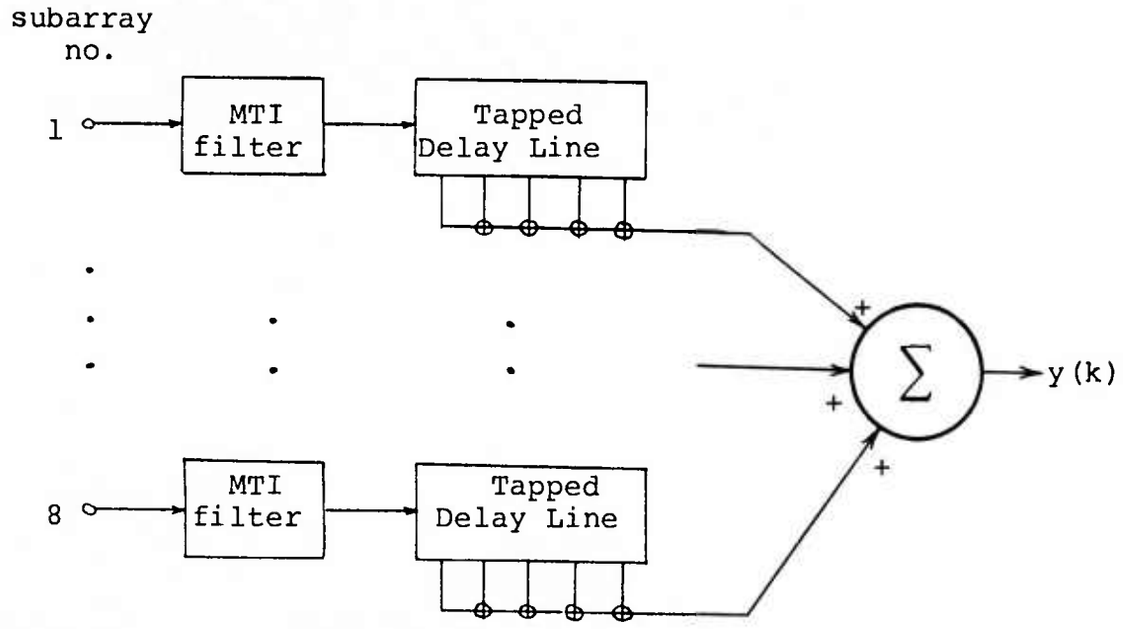

Fig. 13. Location of digital subarray MTI filters used to process experimental data

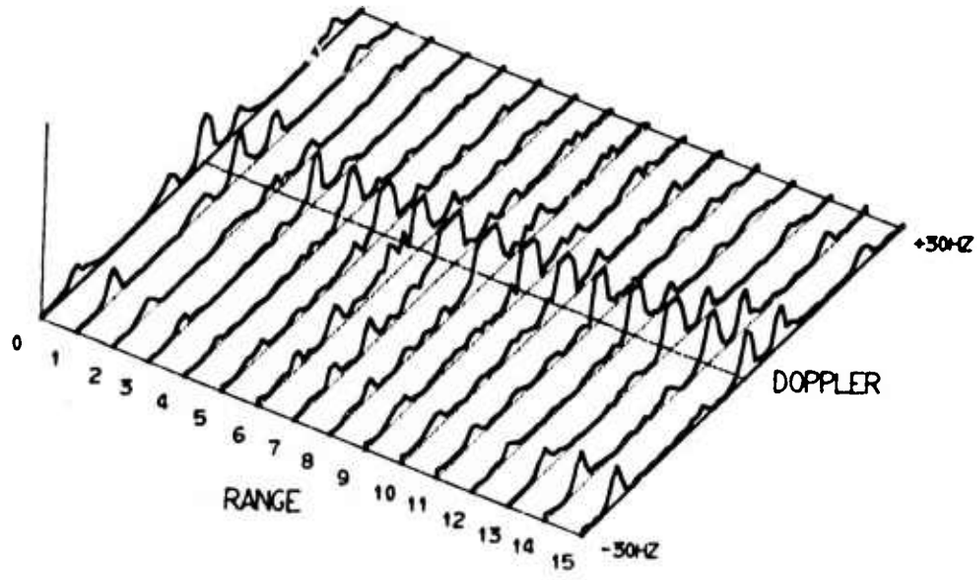

a) No MTI

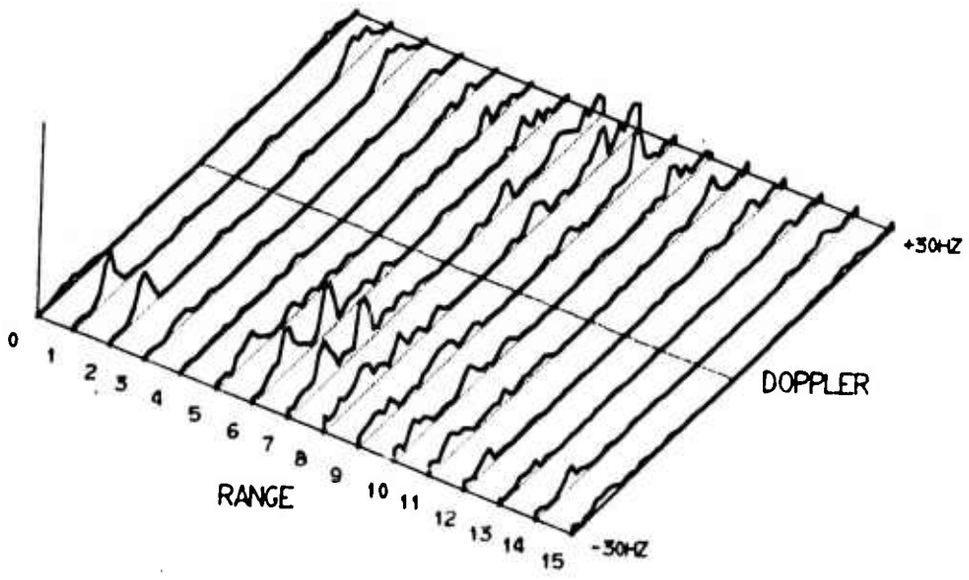

b) Three pulse MTI at each subarray

Fig. 14. Range-doppler map for dwell no. 1 with P-vector processing

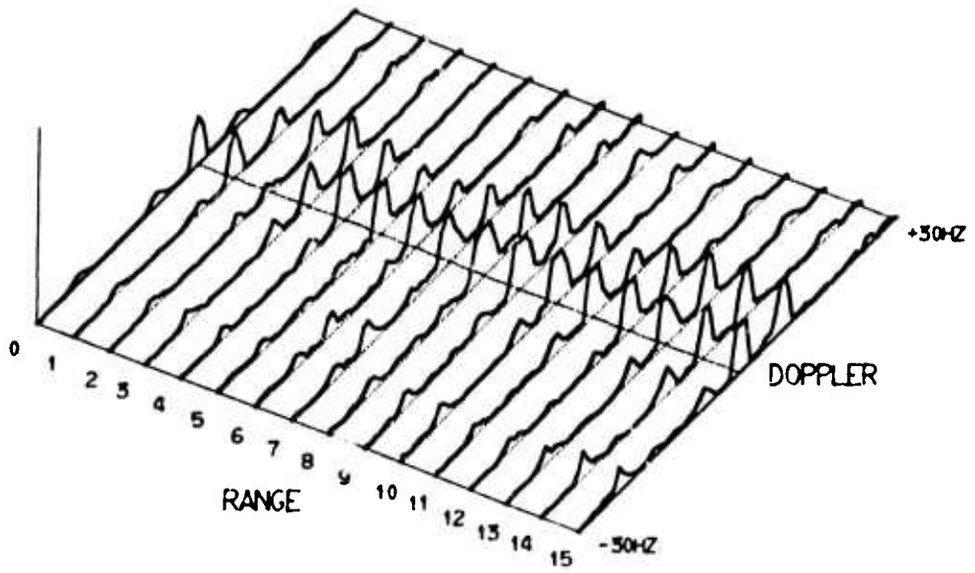

a) No MTI

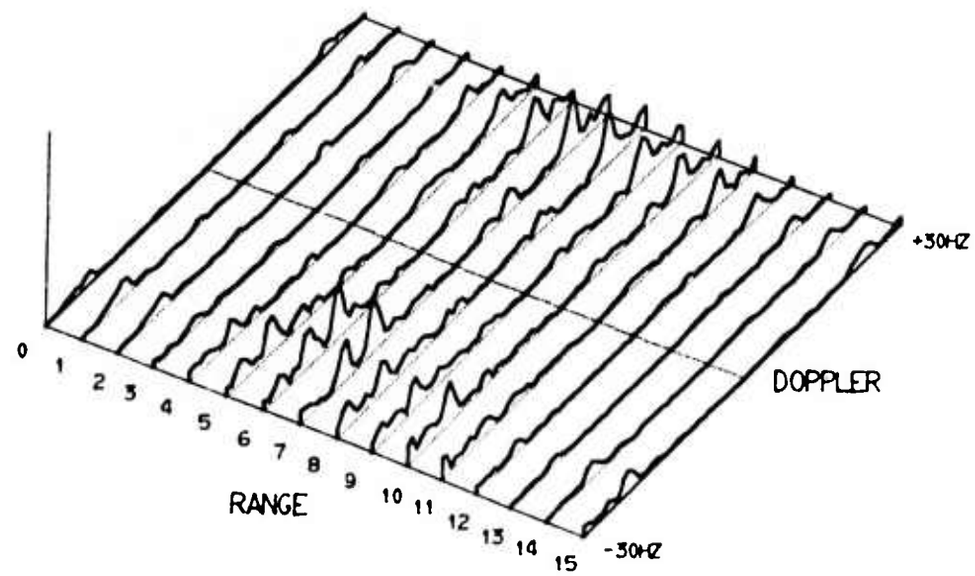

b) Three pulse MTI at each subarray

Fig. 15. Range-doppler map for dwell no. 2 with P-vector processing

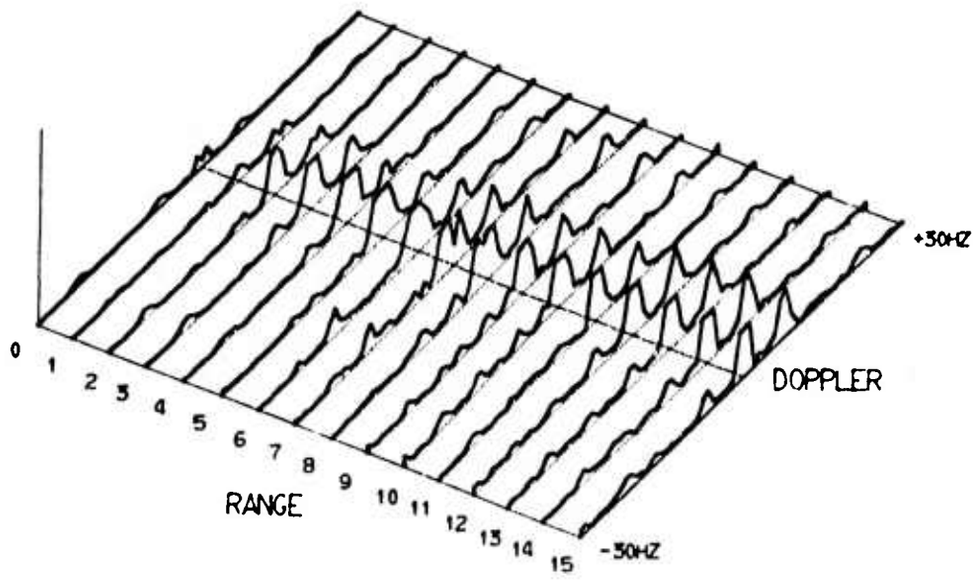

a) No MTI

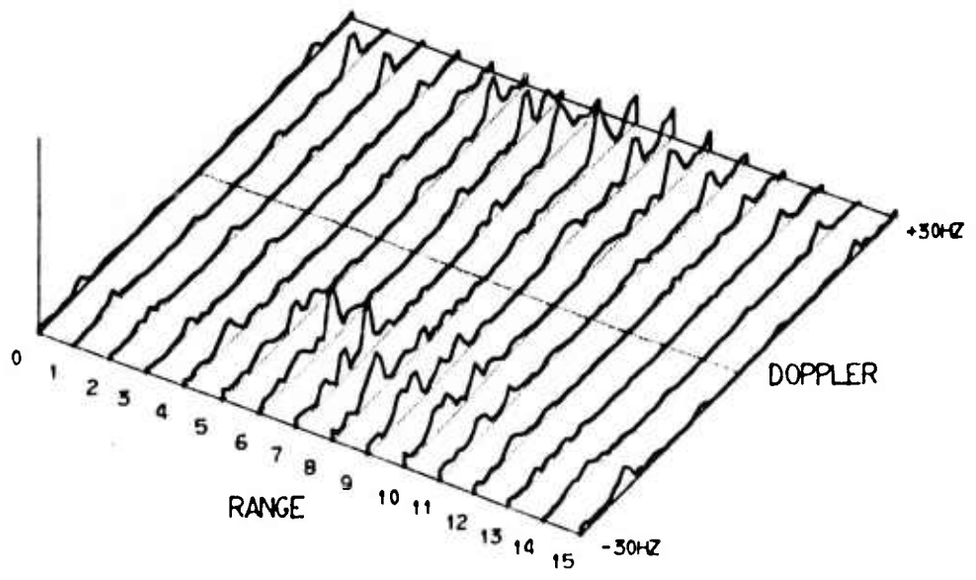

b) Three pulse MTI at each subarray

Fig. 16. Range-doppler map for dwell no. 3 with P-vector processing

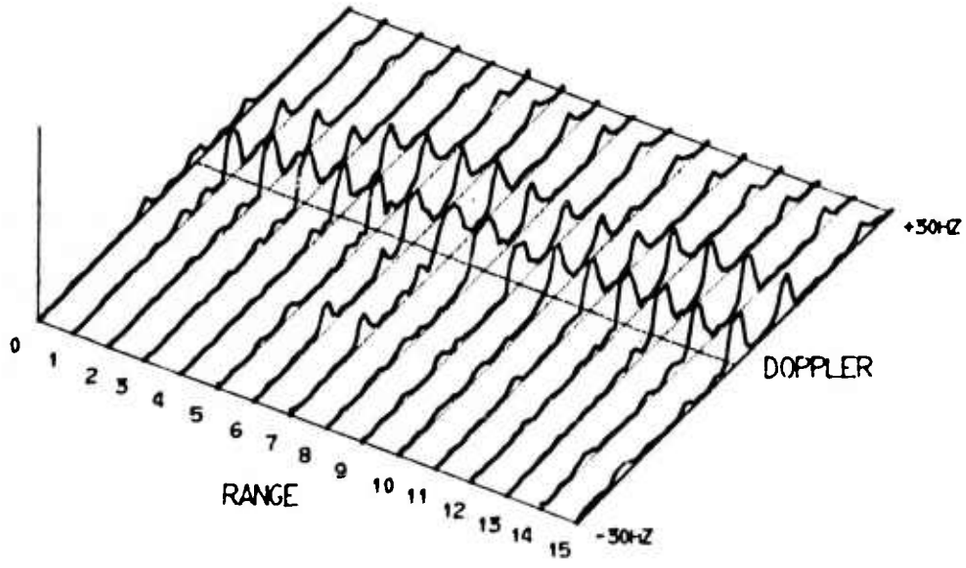

a) No MTI

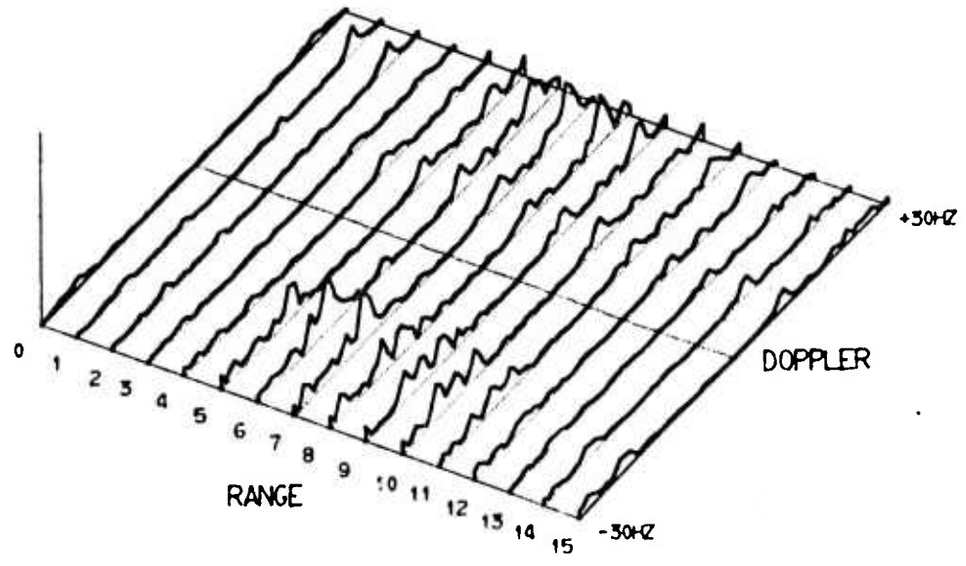

b) Three pulse MTI at each subarray

Fig. 17. Range-doppler map for dwell no. 4 with P-vector processing

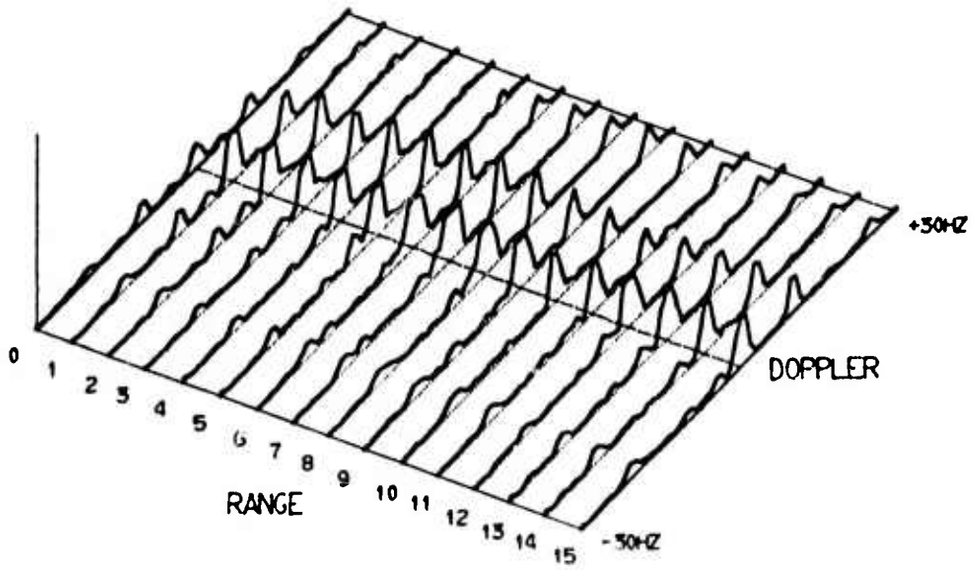

a) No MTI

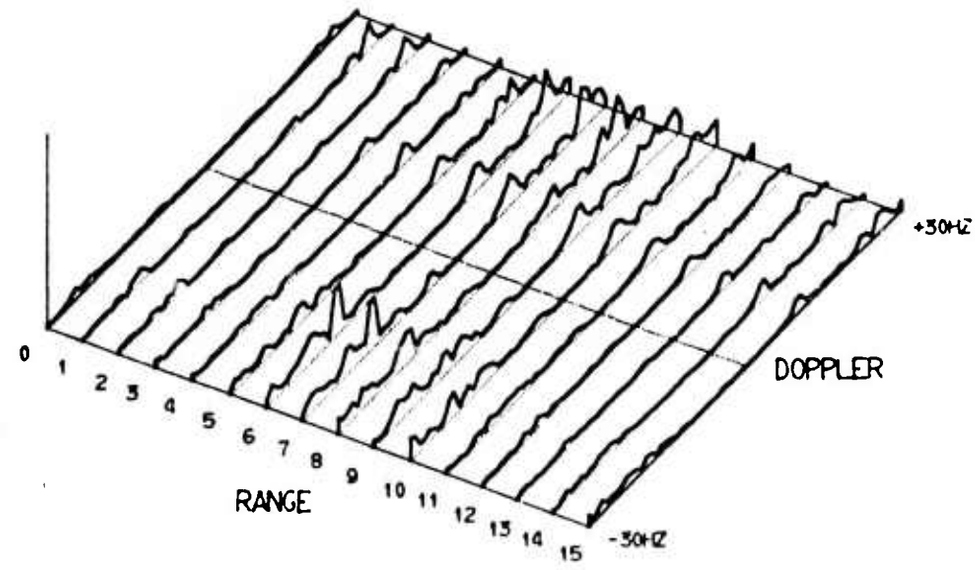

b) Three pulse MTI at each subarray

Fig. 18. Range-doppler map for dwell no. 5 with P-vector processing

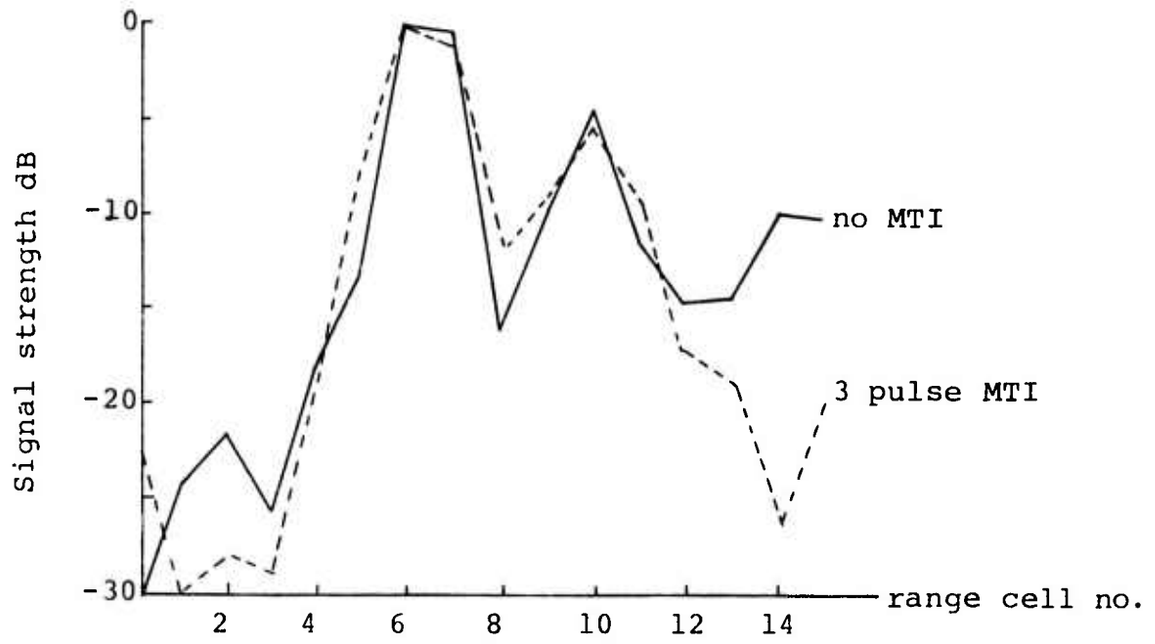

Fig. 19. MTI comparison for dwell no. 3 in doppler bin -17

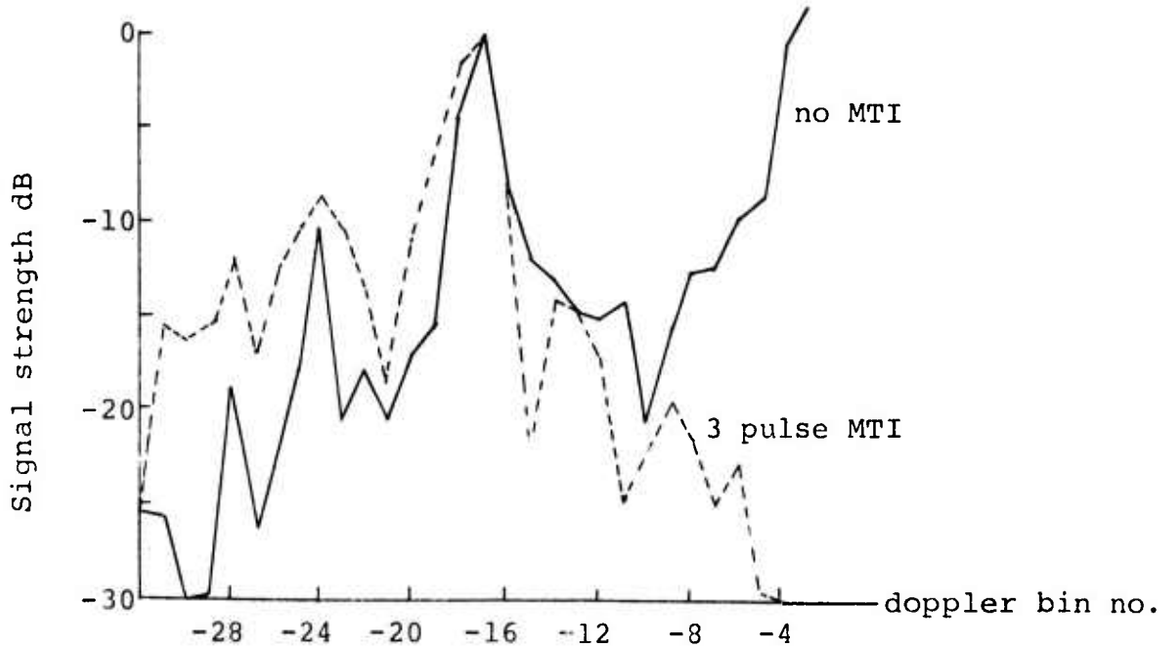

Fig. 20. MTI comparison for dwell no. 3 in range cell 7

with the sections crossing on the target maximum. Finally, signal-to-noise (SNR) and signal-to-interference (SIR) graphs were obtained by extrapolating the noise floor through the target signal and by measuring the peak interference level, respectively. For the case of MTI processing, the interference levels were corrected to account for the 3-pulse MTI filtering function shown in Fig. 12. The results, plotted as a function of dwell number, are given in Figs. 21 and 22. Further discussion of these results is presented in Section VII following.

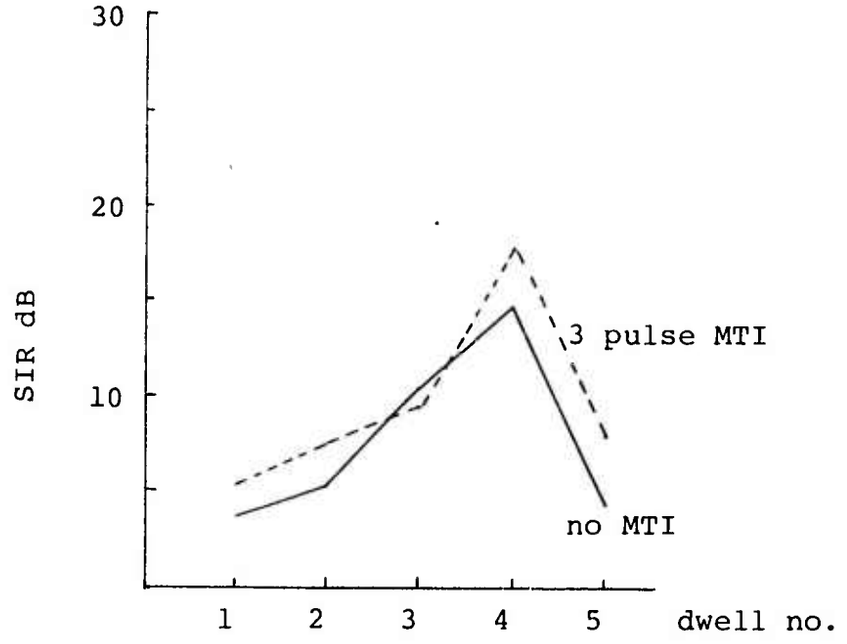

Fig. 21. Signal to interference MTI comparison

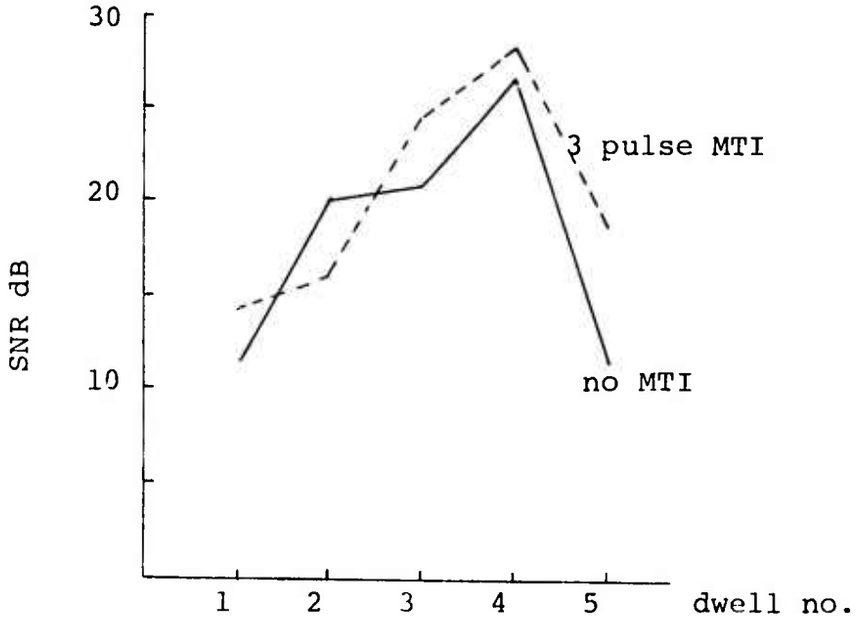

Fig. 22. Signal to noise MTI comparison

V. APERTURE TRADEOFF STUDIES

It is well known that in conventional antenna array processing of planar signals received in an isotropic noise background, increased signal-to-noise ratio can be achieved by increasing the receiving array aperture and maintaining interelement spacing. The amount of the increase is approximately proportional to N, the number of elements in the total array. Clearly, the increase in received SNR cannot proceed indefinitely as elements are added to increase the receiver aperture. The upper bound on output SNR is limited by the spatial coherence length of the signal waveform. It has been demonstrated [9] that at HF, coherence lengths of 15 km or greater can be realized for one-hop ionospheric propagation provided that mode separation methods are available. For the FM-CW transmitter format used in the present studies, mode separation is achieved by frequency filtering and large receiving array apertures can be utilized.

Because the noise background at HF is highly non-isotropic, it is of interest to study aperture/output SNR tradeoffs for the case of signals received in the presence of directional interference. It is, in fact, the non-isotropic nature of the interference environment which allows an adaptive beamformer to provide increased output SNR over that provided by conventional beamforming. Under conditions of high levels of received interference, it is conceivable that an adaptive beamformer would have an output SNR which is less sensitive to the aperture length than a conventional beamformer. To illustrate this property, consider the simple case of a linear,

equally spaced array of N isotropic elements spaced by one-half wavelength. The k^{th} sample of the signal received by the i^{th} element is modeled as $x_i(k)$

$$x_i(k) = n_i(k) + s(k) + d(k - i\Delta) \tag{19}$$

where $n_i(k)$ is white isotropic noise, assumed to be independent from element to element, $s(k)$ is the desired signal (sinusoidal) arriving on boresight and $d(k - i\Delta)$ is a sinusoidal interference, at the same frequency as $s(k)$ but incident at an angle θ which provides a relative time delay of Δ seconds between adjacent elements. The assumed power levels of $n_i(k)$, $s(k)$ and $d(k - i\Delta)$ are σ_n^2, σ_s^2, and σ_d^2, respectively, at each of the N receiving elements.

We consider the case of a beamformer which uses amplitude shading only at each element. Thus, if w_i is the weight at the i^{th} element, the beamformed output signal $y(k)$ is

$$y(k) = \sum_{i=0}^{n-1} w_i\, n_i(k) + w_i\, s(k) + w_i\, d(k - i\Delta). \tag{20}$$

Assuming independence of noise, signal and interference, the out put power $E[y^2(k)]$ may be expressed as a sum of a white noise component, desired signal component and interference component,

$$E[y^2(k)] = \sigma_n^2 \sum_{i=0}^{n-1} w_i^2 + \sigma_s^2 \sum_{i=0}^{n-1} w_i + \sigma_d^2 \left| \sum_{i=0}^{n-1} w_i e^{-j\Delta i} \right|^2 \tag{21}$$

The conventional beamformer which is optimal for the case of isotropic noise only is achieved by setting all weights to the same

value. Since SNR values are unaffected by scale changes in the weights, a normalizing value providing $\sum_{i=0}^{n-1} w_i = 1$ was used for convenience. Thus, with $w_i = \frac{1}{N}$, Eq. (21) for the conventional processor becomes

$$\text{conv } E[y^2(k)] = \frac{\sigma_n^2}{N} + \sigma_s^2 + \frac{\sigma_d^2}{N}\left|\sum_{i=0}^{n-1} e^{-j\Delta i}\right|^2 \qquad (22)$$

The ratios of signal to isotropic noise (SNR), signal to interference (SIR) and signal to total noise (STR) observed at the output of the conventional processor are then given by

$$\text{SNR} = \frac{N\sigma_s^2}{\sigma_n^2}$$

$$\text{SIR} = \frac{N\sigma_s^2}{\sigma_d^2\left|\sum_{i=0}^{n-1} e^{-j\Delta i}\right|^2} \qquad (23)$$

$$\text{STR} = \frac{N\sigma_s^2}{\sigma_n^2 + \sigma_d^2\left|\sum_{i=0}^{n-1} e^{-j\Delta i}\right|^2}$$

A representative plot of these ratios, as a function of N is shown in Figure 23 for the case of $\sigma_s^2 = 1.0$, $\sigma_n^2 = 0.1$, $\sigma_d^2 = 2.0$, and $\Delta = 30°$. Note that the SNR is linear in N and that the SIR goes to infinity at N = 12. This corresponds to an aperture such that a null of the conventional pattern lies in the direction of the interference component.

An adaptive beamformer for the same problem was also implemented. In this case, the amplitude weights w_i used for each element

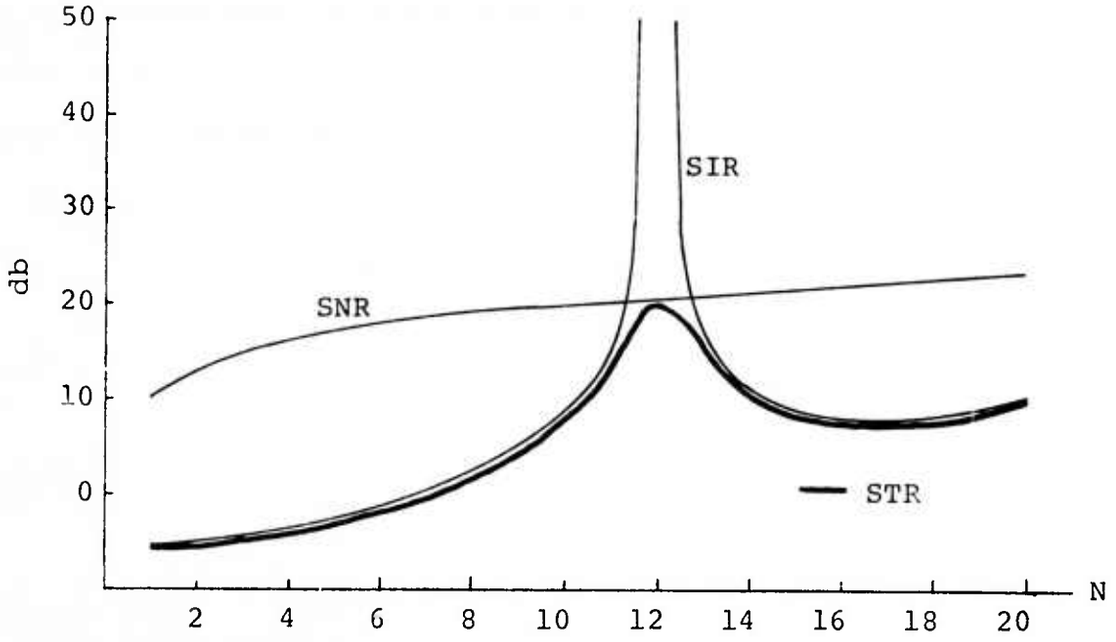

Fig. 23. Signal strength vs. aperture size, conventional processing

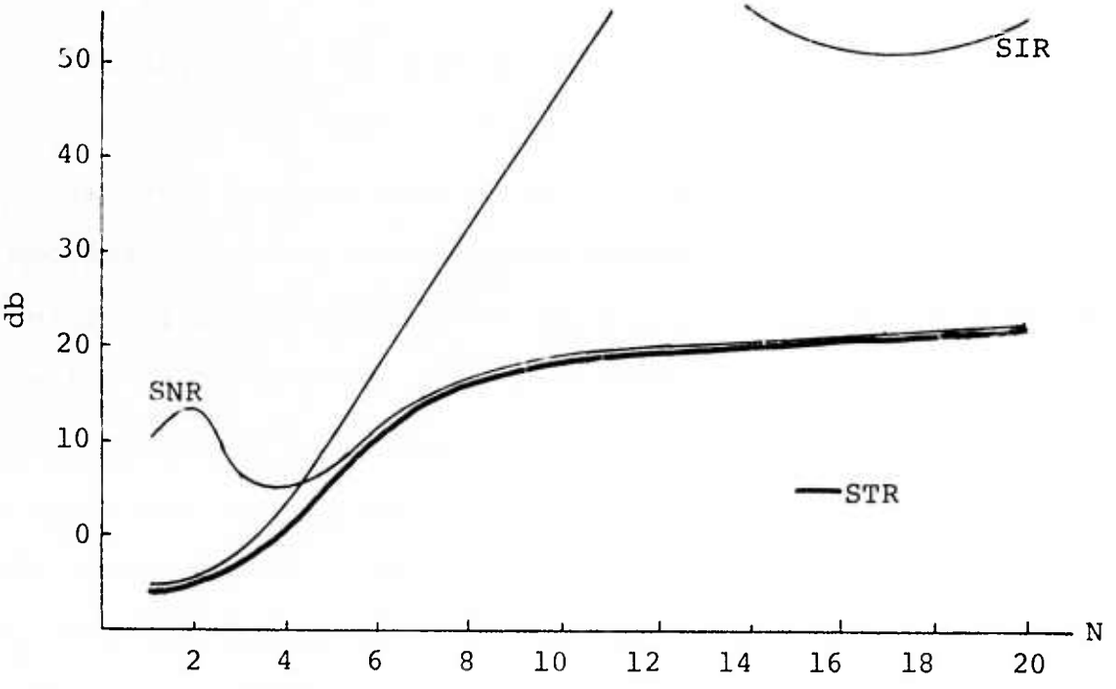

Fig. 24. Signal strength vs. aperture size, adaptive processing

output were chosen using a minimum mean-square error criterion. Thus, the vector of weight coefficients W was computed using the optimal solution given by Eq. (3) in Section III above. For the simple model presently under consideration, the autocorrelation matrix R_{XX} and steering vector P are given by

$$R_{XX} = \sigma_n^2 I + \sigma_s^2 11^T + \sigma_d^2 A \tag{24}$$

$$P = \sigma_s^2 1 \tag{25}$$

where 1 is a column vector of one's and A is an NXN matrix in which the (i,j) element is $\cos[\Delta(i-j)]$. The optimal value of W was computed for N ranging from 1 to 20. The appropriate ratios SNR, SIR, and STR were then computed using the individual terms computed in Eq. (21). The results, plotted as a function of the number of elements N, are presented in Fig. 24.

A comparison of Figs. 23 and 24 reveals several pertinent properties relating to the importance of aperture in conventional and adaptive beamformers. Although these results were generated using amplitude taper only, they are representative of the effects which are observed using either tapped-delay-line processing or gain-phase processing. The first observation is that the ratio of desired signal power to undesired signal power, STR, observed at the output of a conventional beamformer does not increase linearly with increasing aperture when the noise is isotropic. While the trend is generally such that increased aperture provides increased STR, there are cases where a reduction in aperture increases this ratio - i.e., for N in the range 12 to 17. The second observation

is that adaptive processing provides a monotonic increase in STR with increasing aperture and that the value of STR achieved very nearly saturates after a certain minimum aperture has been achieved. The reason for the monotonic behavior is simply that as more elements are added, additional degrees of freedom become available for cancelling the directional interference. The saturation effect is caused by the fact that once a certain minimum number of degrees of freedom have been obtained, further reduction in interference power can be achieved only at the expense of increased isotropic power at the output - i.e., compare the first and third terms in Eq. (21). This saturation effect has been observed elsewhere [8] and has been shown to be a function of the absolute isotropic noise power level. That is, when simulations are carried out using values of σ_n^2 lower than that selected for the present example, the saturation effect occurs at a higher value of N and the resulting STR value is also greater. One factor clearly demonstrated by Fig. 24 is that under some conditions, a reduction in aperture may have virtually no effect on output STR for an adaptive processor.

Experimental Aperture Tradeoff Studies

In order to investigate the effect of aperture changes on the performance of an adaptive processor operating in an actual HF signal environment, the data collected on March 15, 1974 and previously shown in Figs. 4 through 8, was processed at less than full aperture. In each case, P-vector adaptation was used with $\alpha = 0.1$ and 5 adaptive coefficients per subarray output. Figure 25 shows

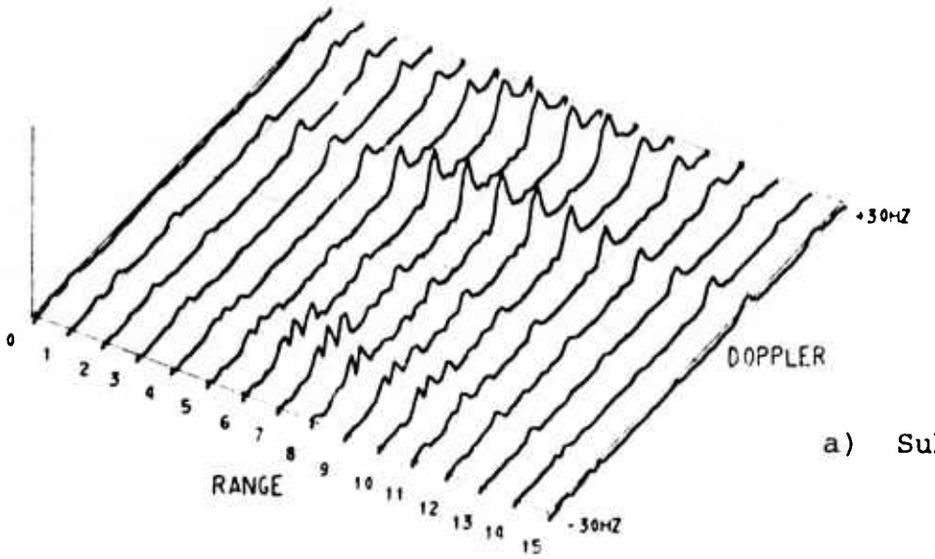

a) Subarrays 1,2

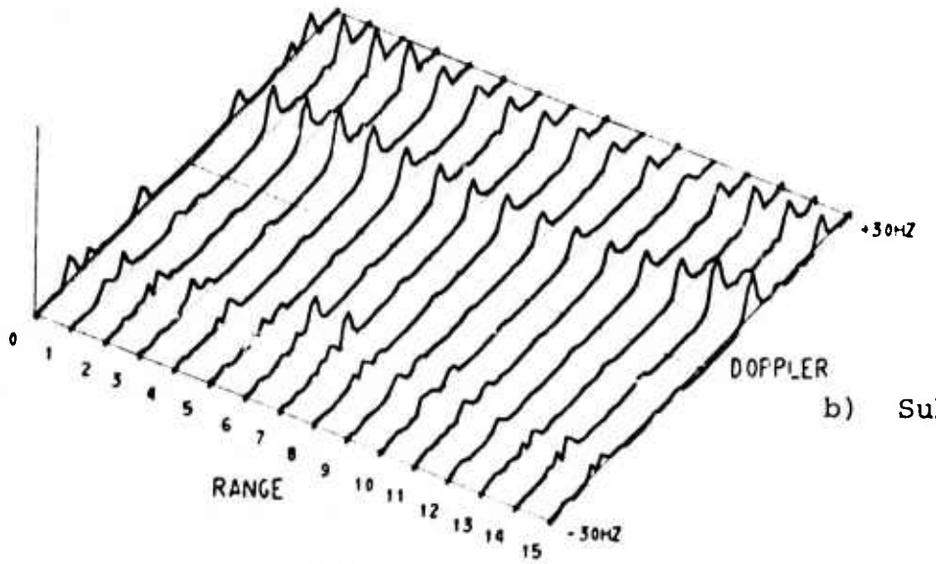

b) Subarrays 1,2,3,4

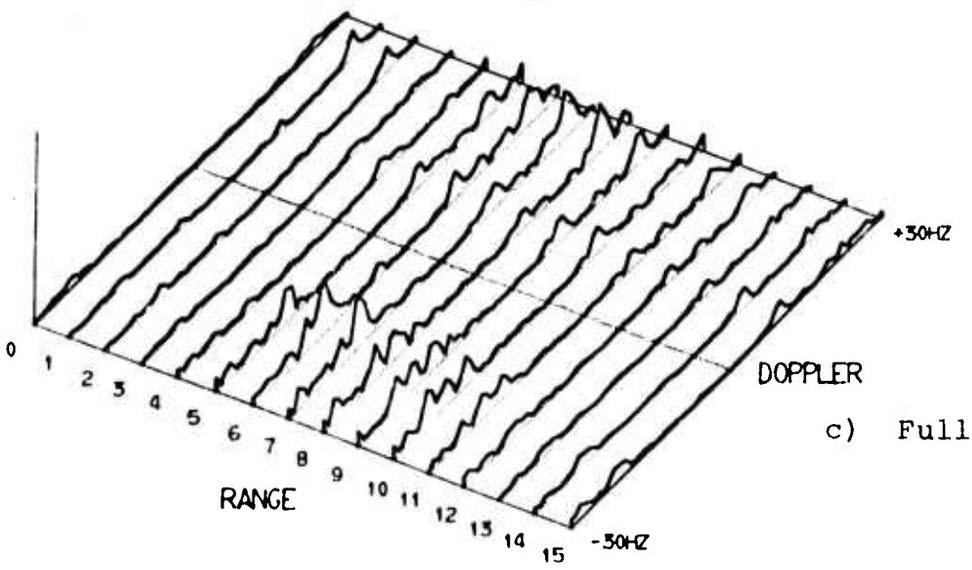

c) Full array

Fig. 25. Aperture trade-off comparison for dwell no. 4 using P-vector adaptation with $\alpha=0.1$

results obtained during dwell No. 4 with 3-pulse MTI in use. The three plots represent processing of the same data values with two adjacent subarrays (Fig. 25a), four adjacent subarrays (Fig. 25b), and the full array of eight subarrays (Fig. 25c).

Comparison of Figs. 25b and c indicates that reduction of the aperture size by a factor of two had little detrimental effect on array performances. Further reduction by an additional factor of two, however, produced significantly inferior results. The effects of aperture were further studied by varying the aperture size while maintaining the number of subarrays at two. Figure 26 shows results obtained using two adjacent subarrays, two at half aperture and two at the full aperture. The two at half aperture illustrate a clear advantage over any other aperture. This effect was not restricted to adaptive processing, as illustrated in Fig. 27. In this case, the same data were processed using a conventional beamformer. Again, the superiority of the half aperture configuration is apparent. The effect was also not observed on only one dwell but occurred frequently throughout the data record. Figure 28 illustrates a similar effect obtained using the adaptive processor on dwell no. 3.

One possible explanation for this effect is the presence of a fading null across the array. Since the scale size of HF fading structures is known to be smaller than the Los Banos aperture, it is possible that several of the subarrays were resident in a fading null during these tests. It is clear that the problem of aperture tradeoffs in the HF environment is not a simple one and further study of these effects is warranted. The phenomenon illustrated in

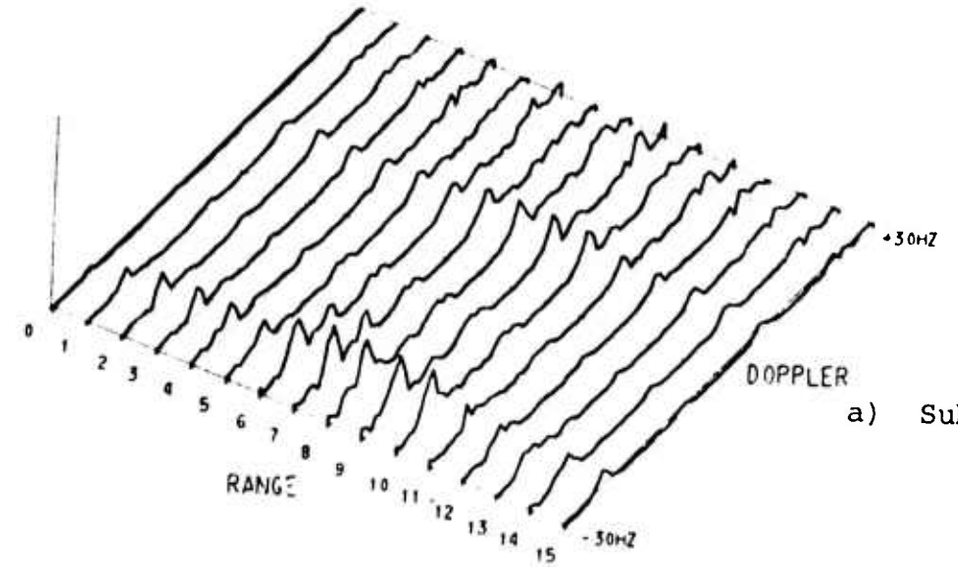

a) Subarrays 1,2

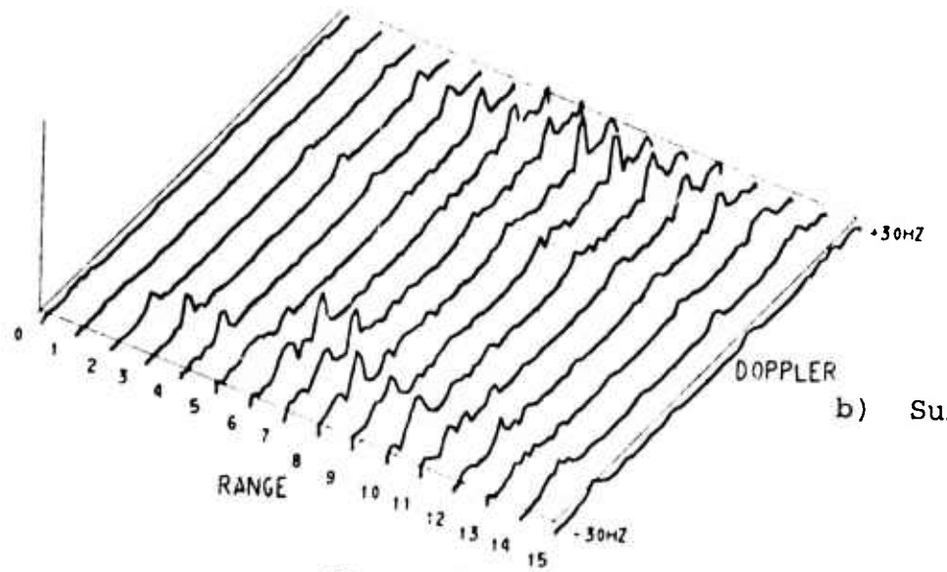

b) Subarrays 1,4

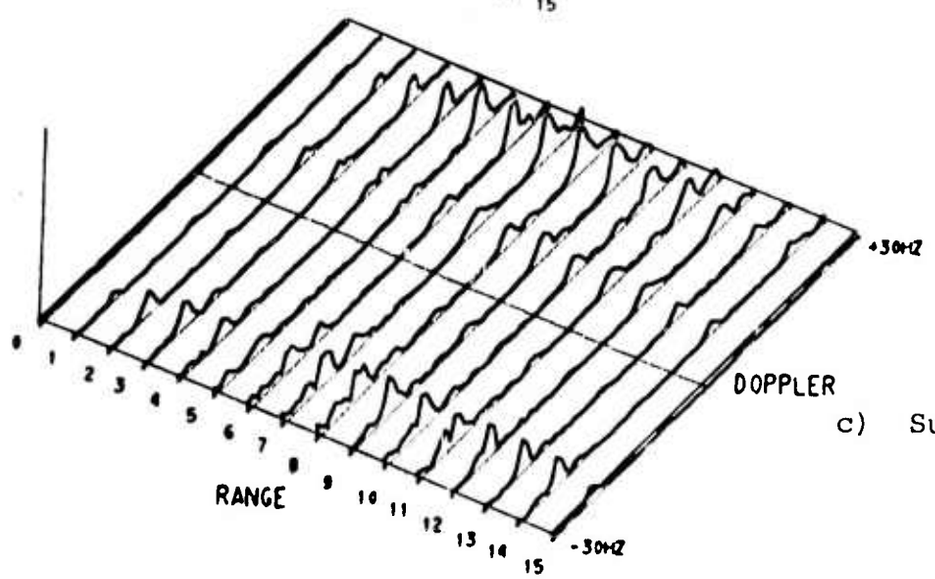

c) Subarrays 1,8

Fig. 26. Aperture trade-off comparison using two subarrays on dwell no. 2 and P-vector adaptation, α=0.1

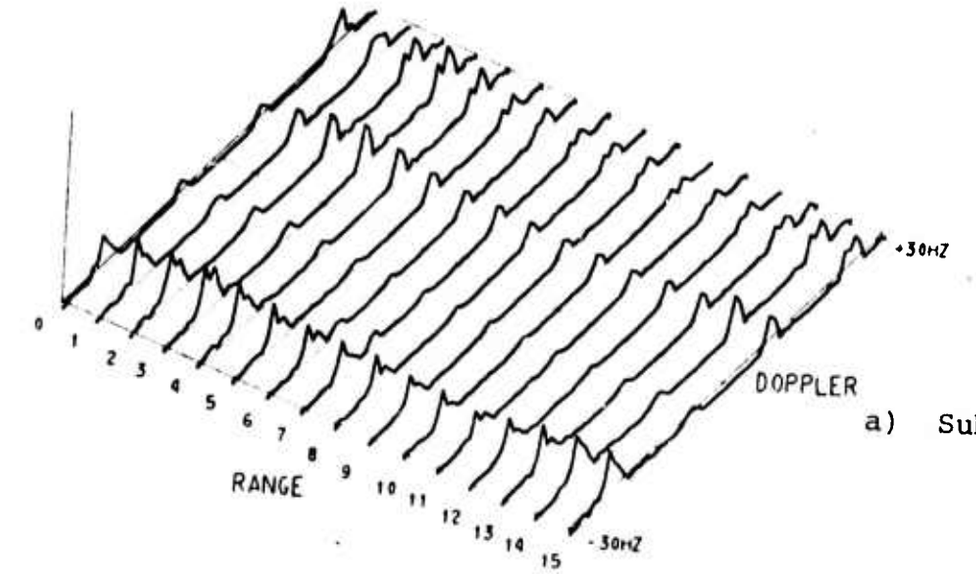

a) Subarrays 1,2

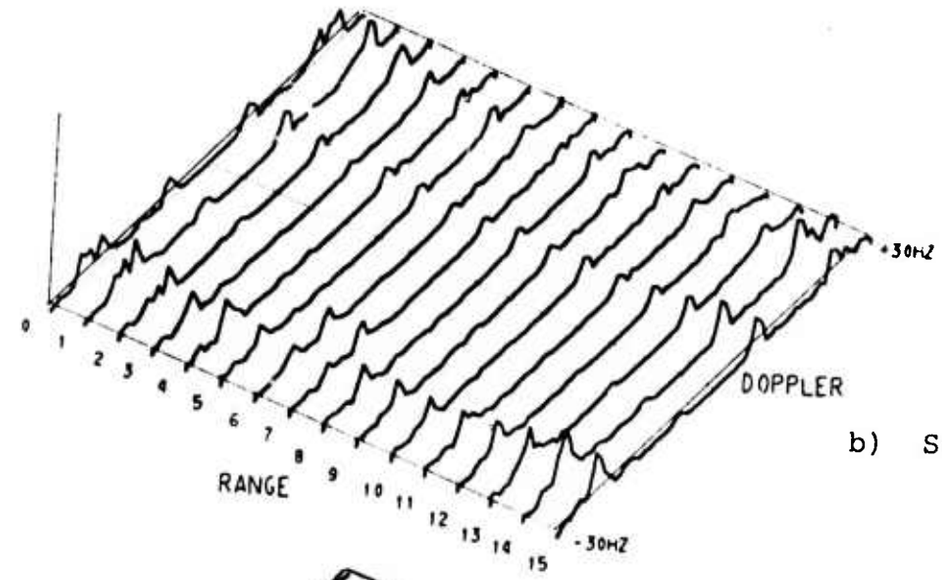

b) Subarrays 1,4

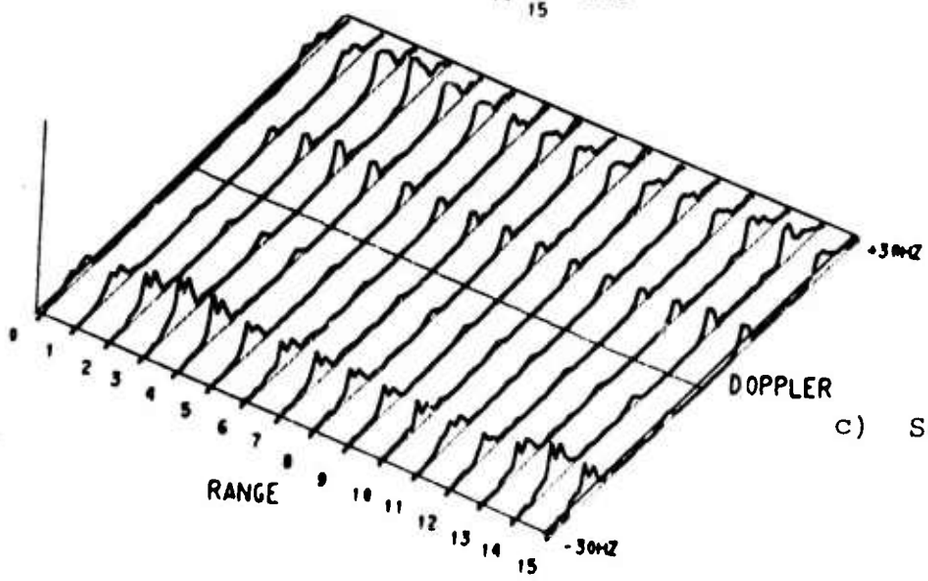

c) Subarrays 1,8

Fig. 27. Aperture trade-off comparison using two subarrays on dwell no. 2 and conventional processing

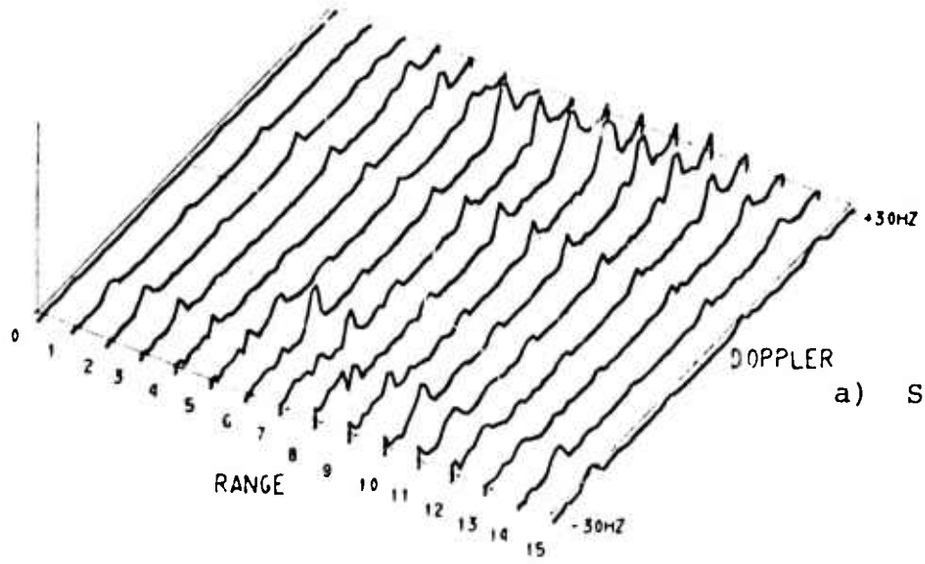

a) Subarrays 1,2

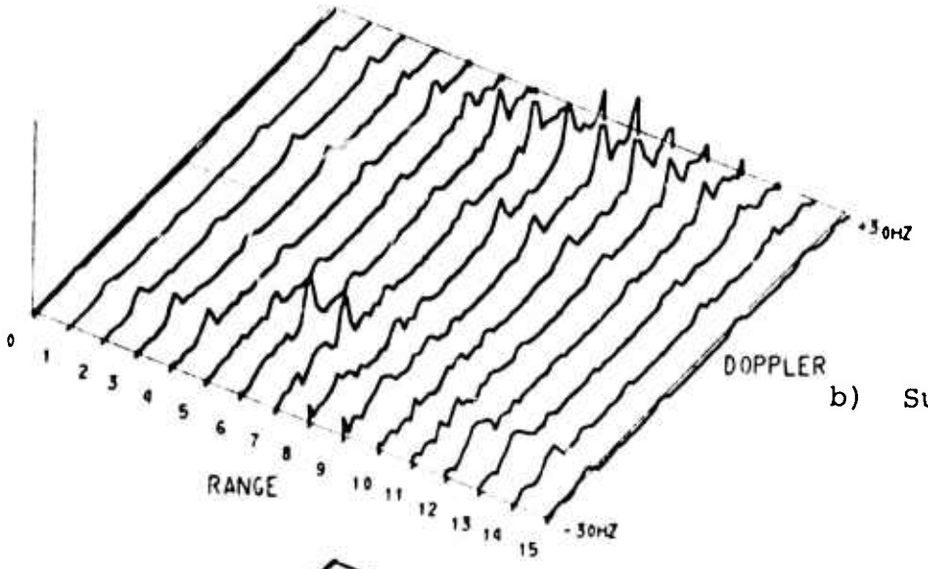

b) Subarrays 1,4

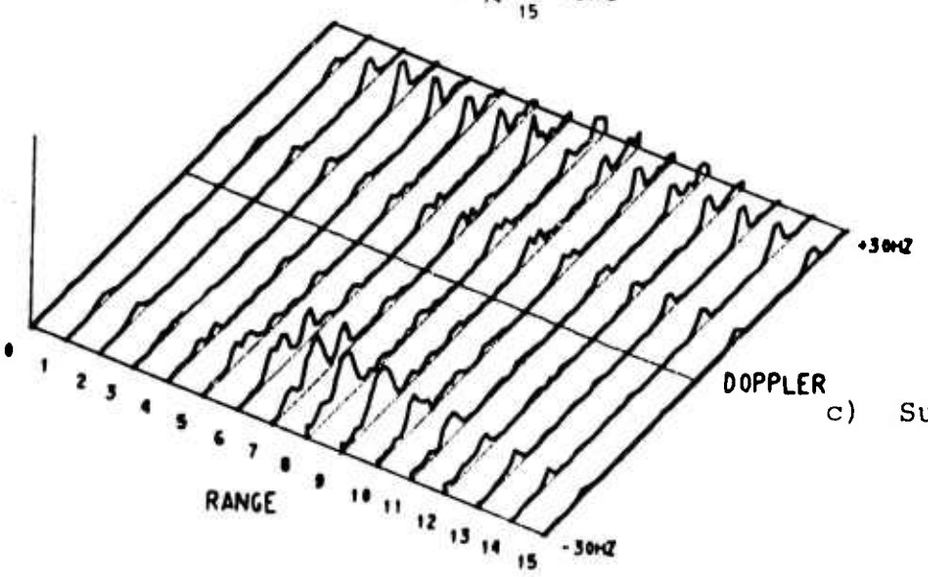

c) Subarrays 1,8

Fig. 28. Aperture trade-off comparison using two subarrays on dwell no. 3 and P-vector adaptation, α=0.1

Figs. 25-28 are further evidence of the advisability of using adaptive processing at HF. Since such effects are most certainly time varying, one advantage offered by adaptation is that of placing greater weight on the high SNR subarray outputs.

VI. MINIMUM MEAN-SQUARE ERROR ADAPTATION WITH LINEAR CONSTRAINTS

The adaptive beamforming method used to process data in this and previous [2,3] reports has been referred to as the P-vector adaptation algorithm. A complete description of this algorithm, including its derivation and convergence properties, has been presented elsewhere.[10] Briefly, the procedure is designed to minimize the mean-square error between a desired signal d(k), which is presumed to be incident on the array from a known direction. For the FM/CW backscatter radar case, the desired response is assumed to be sinusoidal with a frequency ω_0 determined by the range of interest. Thus, the desired response is

$$d(k) = \cos(\omega_0 k) \tag{26}$$

and the signal observed at the sampled output of the i^{th} subarray is assumed to be of the form

$$X_i(k) = A_i d(k-\tau_i) + n_i(k) \tag{27}$$

where $n_i(k)$ is the sum of all noise and interference components at the i^{th} subarray output. Under these assumptions, the beamformed output signal, y(k) [Eq.(1)], can be expressed as a sum of desired and noise components,

$$Y(k) = Y_d(k) + Y_n(k) \tag{28}$$

The P-vector algorithm, Eq's (2) and (5), is then designed to adapt toward a set of weighting coefficients which minimize the

mean-square difference $E[\varepsilon^2(k)]$ between $d(k)$ and $Y(k)$, i.e.

$$E[\varepsilon^2(k)] = E[\{d(k) - Y(k)\}^2] \tag{29}$$

The optimum vector of coefficients W^* which minimizes (29) is given by Eq. (3) and is referred to as the constraint-free, minimum mean-square error beamforming solution. One significant property of this solution is that the resulting array processor may provide frequency-domain filtering of signals received from the desired direction. An example of this filtering is illustrated in Figure 29. This two-dimensional plot shows the array pattern response at 16 resolvable azimuths, labeled 0 through 15, as a function of frequency within the receiver bandwidth, 0 to 960 Hz. The plot was obtained using a two-dimensional Fourier Transform[4] of coefficients generated by use of the P-vector adaptation algorithm on data recorded September 3, 1974. Eastward transmissions were employed and the beamformer consisted of five coefficients per subarray with $\alpha = 0.1$. MTI processing was not in use for this test. The desired direction of arrival corresponded to azimuth cell number 8 and the desired frequency was 480 Hz, as shown by the arrow.

Note that any signal incident on the array from the desired direction and at the desired frequency is in the main lobe of the pattern. In addition, a variety of nulls, extending in both frequency and azimuth, are evident. The location and nature of these nulls is a reflection of the noise and interference environment under which data were recorded. A variety of similar plots, taken under many other data configurations, are presented in a recent SRI report.[4]

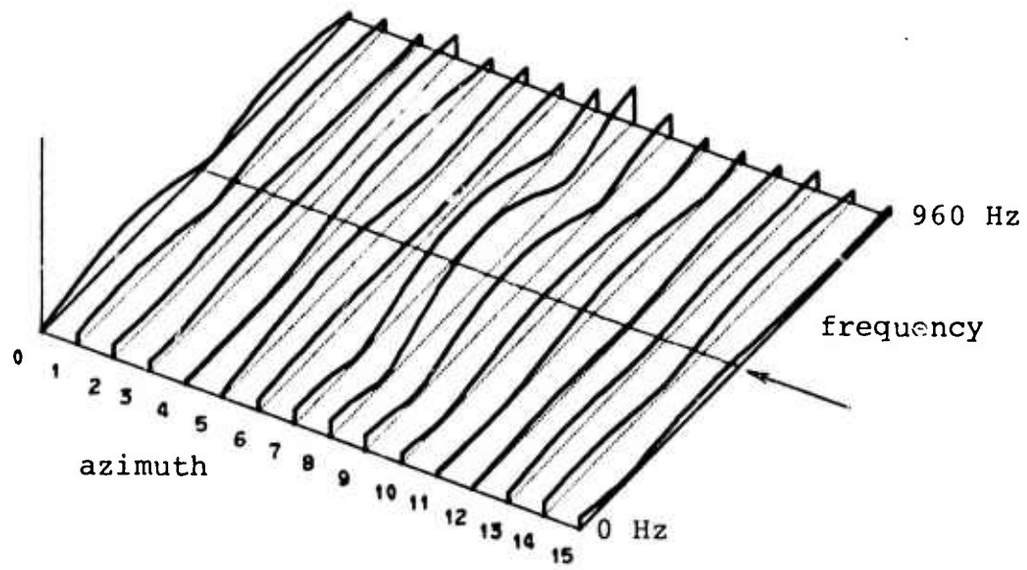

Fig. 29. Azimuth-frequency response for P-vector adaptation algorithm on data recorded September 3, 1974

Inspection of Fig. 29 reveals that signals which are incident on the array from the desired direction, but at a frequency other than the desired 480 Hz value, will be attenuated with respect to the response at 480 Hz. In the range-doppler display, frequency tapering of this type appears as range-dependent filtering. Examination of the interference lines in the adaptive plots presented earlier, Figs. 4 through 8, shows further evidence of this effect. It is to be noted, however, that the frequency (or range) filtering is never particularly sharp for the filter parameters used in this study and will not, for example, modify an interference line to the point of making it appear target-like. The sharpness of this filtering is increased as the number of adaptive coefficients per subarray output is increased. With five taps, the effective minimum bandwidth of the filter is approximately 6.5 range lines. Extending the processor to 16 taps per subarray would reduce the bandwidth to two range lines and might very well cause interference to appear target-like in the range-doppler display.

It is possible to derive optimal beamforming procedures which are constrained to have a flat frequency response in the desired look direction of the array, regardless of the number of taps used to process each subarray output. Such procedures fall into a class termed minimum mean-square error with constraints and have been studied extensively by previous authors.[11-13] Of particular interest is a recent procedure suggested by Frost[5] which allows time-domain adaptation under linear constraints. In the sections following a brief description of the optimal

processor and Frost's algorithm are presented. Comparative experimental results obtained using both P-vector and Frost adaptation on the same data are also given.

Optimum Constrained Least-Mean Squares Filter Coefficients

The constrained minimum-mean square error beamformer is designed to minimize the total array output power subject to a linear constraint on the filter coefficients. (Clearly, with no such constraint, the optimum solution is obtained by setting all coefficients to zero.) With reference to the weight vector defined in Eq. (6), the constraint may be expressed as

$$C^T W = F \tag{30}$$

where W is the K-L dimensional vector of weights for a processor containing K subarrays and L taps per subarray; C and F are, respectively, a J by KL matrix and a J-dimensional vector of known constants which determine the constraints. In effect, Eq. (30) is a specification of $J < KL$ simultaneous constraint equations on the weight vector.

For array processing with a frequency independent main lobe, the appropriate constraint is that the sum of K coefficients taken across the array after any number of identical delays should be zero except for one pre-specified delay value, which has a sum of unity. Mathematically, for the 8 subarray, 5 tap per subarray case, this is expressed as

$$\sum_{i=1}^{8} w_{ij} = 0 \qquad j = 0,1,3,4$$

$$\sum_{i=1}^{8} w_{i2} = 1 \tag{31}$$

With this constraint, any signal which arrives on boresight is received by all eight subarrays simultaneously and therefore appears undistorted at the output when it reaches tap no. 2. Note that the processor requires time delay beamsteering prior to processing to provide an effective boresight desired look direction.

The equivalent C and F matrices in (30) for this constraint are given by

$$C = \begin{bmatrix} 1 & 0 & \cdot & \cdot & 0 \\ 1 & 0 & \cdot & & \cdot \\ \cdot & \cdot & \cdot & & \cdot \\ 1 & 0 & & & \cdot \\ 0 & 1 & 0 & & \cdot \\ \cdot & 1 & & & \cdot \\ \cdot & \cdot & & & \cdot \\ 0 & 1 & 0 & & \cdot \\ 0 & 0 & \cdot & & \cdot \\ \cdot & \cdot & \cdot & & 1 \\ \cdot & \cdot & & & \cdot \\ 0 & 0 & \cdot & \cdot & 1 \end{bmatrix} \tag{32a}$$

(dimension markings: 8 rows per block; 40 rows total; 5 columns)

$$F = \begin{bmatrix} 0 \\ 0 \\ 1 \\ 0 \\ 0 \end{bmatrix} \tag{32b}$$

The optimum weight vector W* which minimizes $E[y^2(k)]$ subject to the constraint (30) is

$$W^* = R_{XX}^{-1}C[C^T R_{XX}^{-1}C]^{-1}F \tag{33}$$

It can be shown[12] that this solution is closely related to the unconstrained minimum mean-square error solution given by Eq. (3) when C and F have the form in (32). In particular, the unconstrained solution has been shown to have, in general, a higher output signal-to-noise ratio than does the constrained method. In the limit of arbitrarily high input signal to total noise ratio, however, the two processors become virtually identical. Qualitatively, the lower STR in the constrained case is due to the fact that some of the adaptive degrees of freedom are taken up by the constraint. The extreme example of this would occur when the number of constraints was set equal to the number of coefficients. Thus in Eq. (30) with J=KL, the matrix C is square and, if non-singular, completely determines the weight values, irrespective of the data received by the array.

Constrained Least-Mean Square Adaptation

Frost[5] has presented a time-domain adaptation procedure

which may be used to adapt toward the optimal solution defined by Eq. (33). The method is similar to the P-vector algorithm in that the processor coefficients are updated as each new sample of data is received and measurement of signal correlation matrices are not required. Frost's algorithm has the additional advantage that it is self-correcting and avoids error accumulation while maintaining the specified constraint. Roundoff and truncation errors thus have a minimal effect upon the performance of the algorithm.

For the general constraint conditions defined by Eq. (30), Frost's procedure may be expressed as

$$W(k+1) = Q[W(k) - \mu y(k)X(k)] + F \tag{34}$$

where Q is a square KL by KL matrix of known coefficients,

$$Q = I - C(CC^T)^{-1}C^T \tag{35}$$

and W(k) and X(k) are the coefficient and signal vectors defined by Eq.'s (6) and (7) above. When the C matrix has the particularly simple form shown in Eq. (32a), the premultiplication by Q in (34) can be expressed in terms of additions as follows:

$$w_{1,0}(k+1) = w_{1,0}(k) - \mu y(k)X_1(k) - \frac{1}{8}\left[\sum_{j=1}^{8} w_{j,0}(k) - \mu y(k)X_j(k)\right] + \frac{f_1}{8} \tag{36a}$$

$$\vdots$$

$$w_{8,0}(k+1) = w_{8,0}(k) - \mu y(k)X_8(k) - \frac{1}{8}\left[\sum_{j=1}^{8} w_{j,0}(k) - \mu y(k)X_j(k)\right] + \frac{f_1}{8} \tag{36b}$$

$$w_{1,1}(k+1) = w_{1,1}(k) - \mu y(k)X_1(k-1) - \frac{1}{8}\left[\sum_{j=1}^{8} w_{j,1}(k) - \mu y(k)X_j(k-1)\right] + \frac{f_2}{8} \tag{36c}$$

$$\vdots$$

$$w_{8,4}(k+1) = w_{8,4}(k) - \mu y(k)X_8(k-4) - \frac{1}{8}\left[\sum_{j=1}^{8} w_{j,4}(k) - \mu y(k)X_j(k-4)\right] + \frac{f_5}{8} \tag{36d}$$

The total number of digital operations required to implement these equations on a digital computer for a 40 weight processor is 95 real multiplies and 240 real additions. In the case of P-vector adaptation, the numbers are 81 multiplies and 120 additions. It should be noted that for both processors these values include the 40 multiplies and adds necessary to compute the beamformed output y(k).

Experimental Comparisons

Figures 30 through 34 show a series of successive range-doppler plots obtained using a one-second integration period. In each case, the same data were processed using both P-vector and Frost adaptation methods with five adaptive coefficients per subarray and an α value of 0.1. The data were recorded using eastward looking transmissions on March 15, 1974 and are identical to that shown in Figs. 4-8. MTI filters were not in use during processing.

A comparison of these results illustrates that the received target signal-to-noise and signal-to-interference ratio is generally greater for P-vector adaptation than for adaptation using the Frost procedure. Cross-sectional received signal plots taken at the target doppler frequency as a function of range are shown in Figs. 35 and 36 for dwell no. 3. Also shown for purposes of comparison are the results obtained with conventional processing.

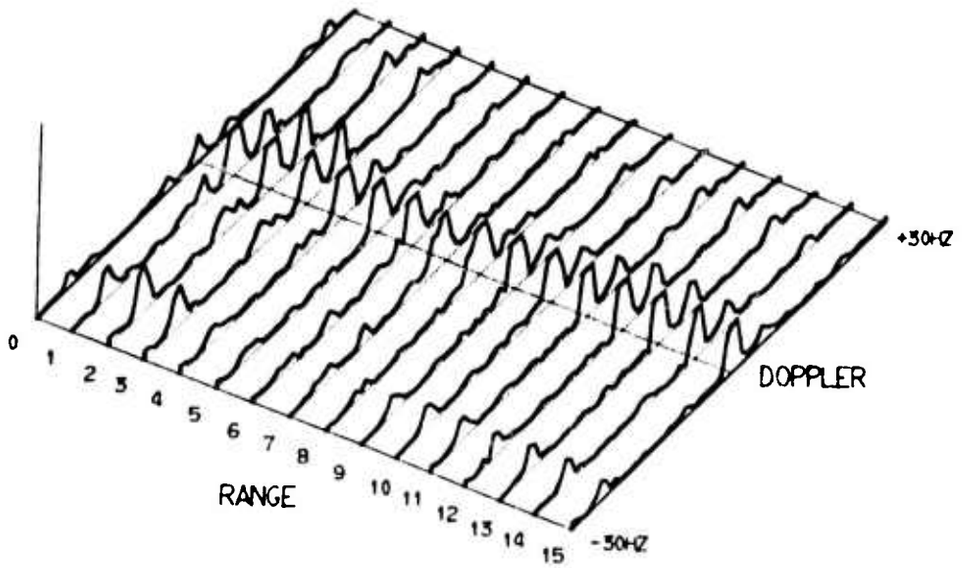

a) Frost algorithm

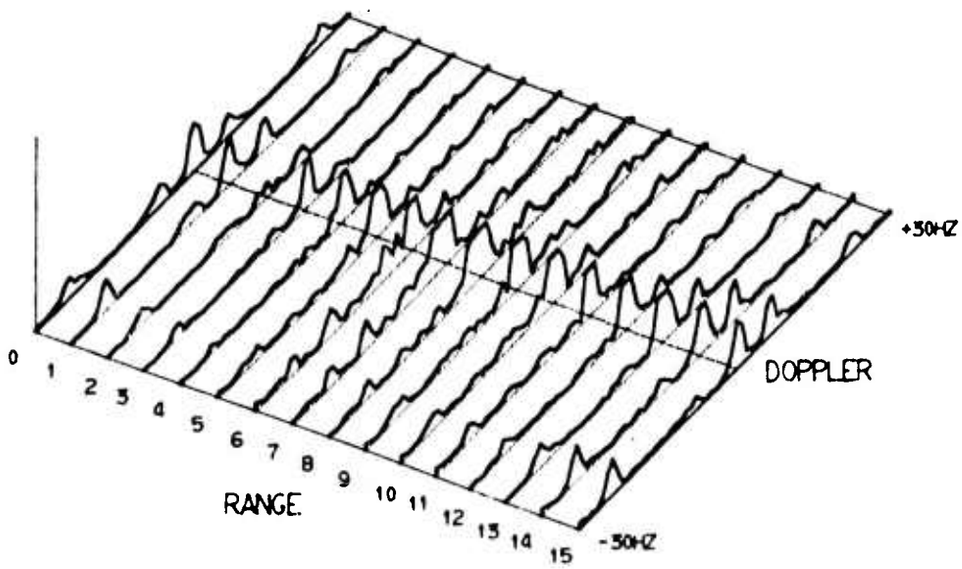

b) P-vector algorithm

Fig. 30. Constrained minimum mean-square error comparison for dwell no. 1, March 15, 1974

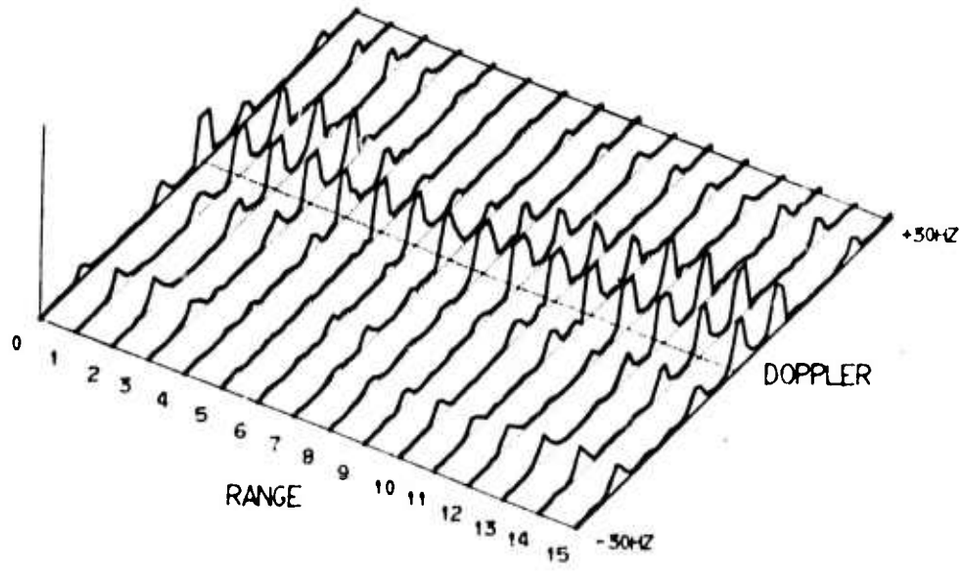

a) Frost algorithm

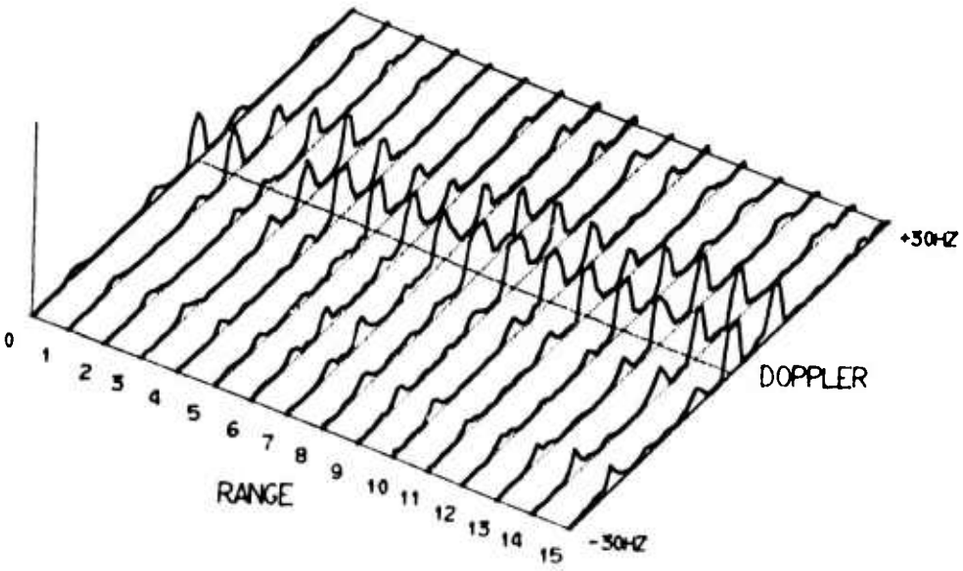

b) P-vector algorithm

Fig. 31. Constrained minimum mean-square error comparison for dwell no. 2, March 15, 1975

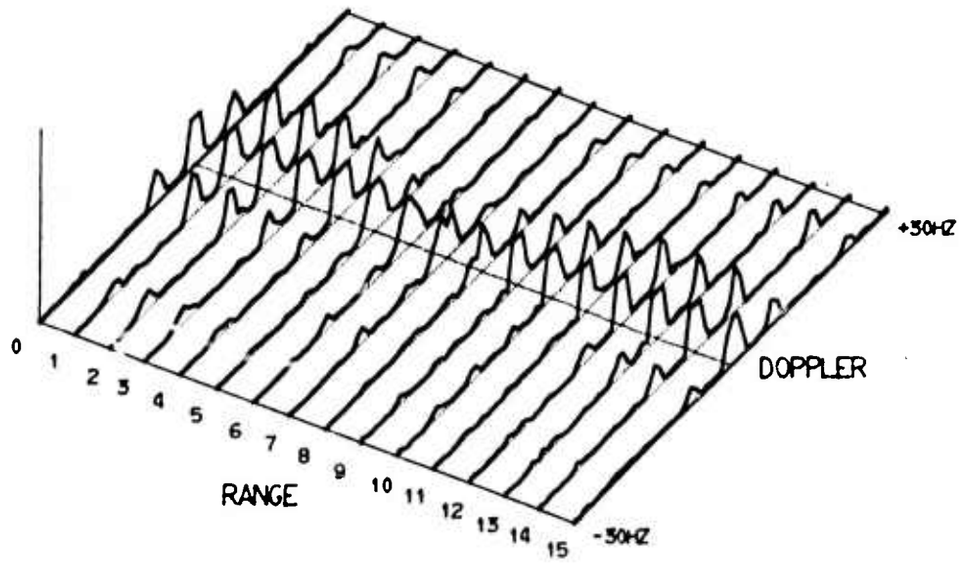

a) Frost algorithm

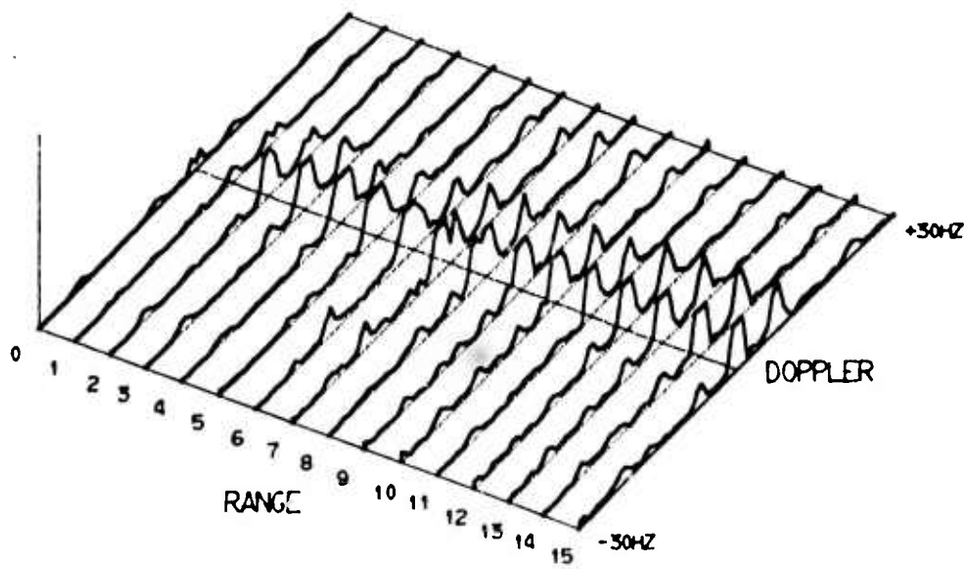

b) P-vector algorithm

Fig. 32. Constrained minimum mean-square error comparison for dwell no. 3, March 15, 1974

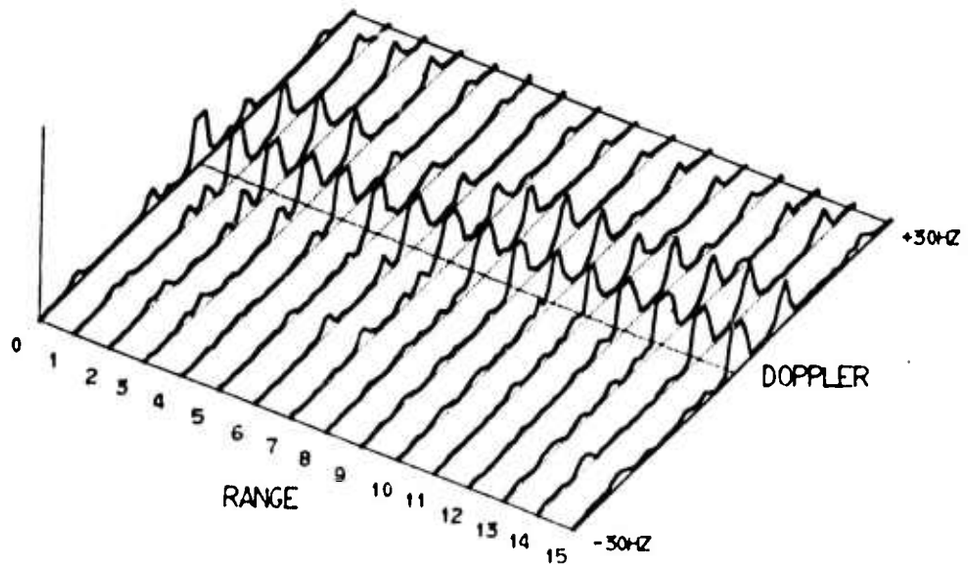

a) Frost algorithm

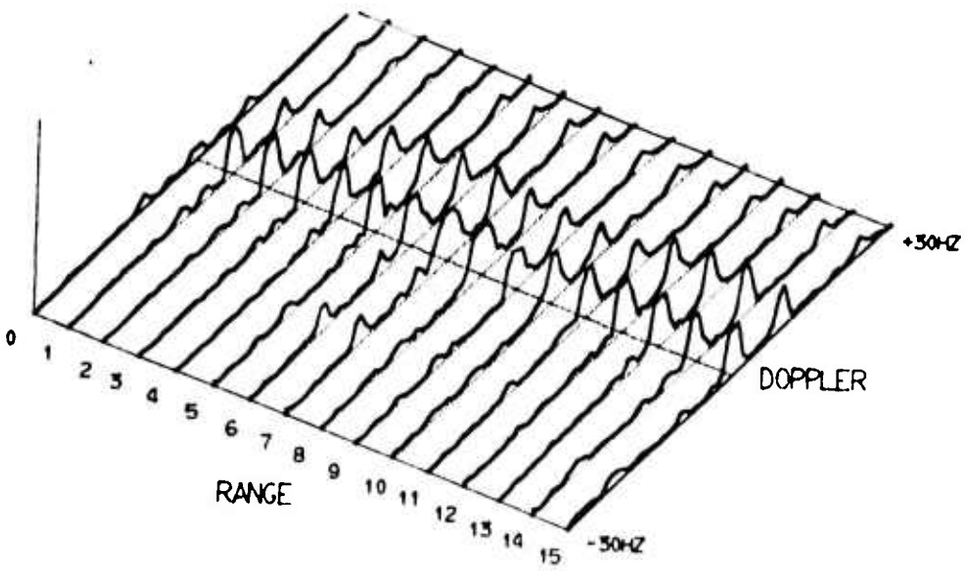

b) P-vector algorithm

Fig. 33. Constrained minimum mean-square error comparison for dwell no. 4, March 15, 1974

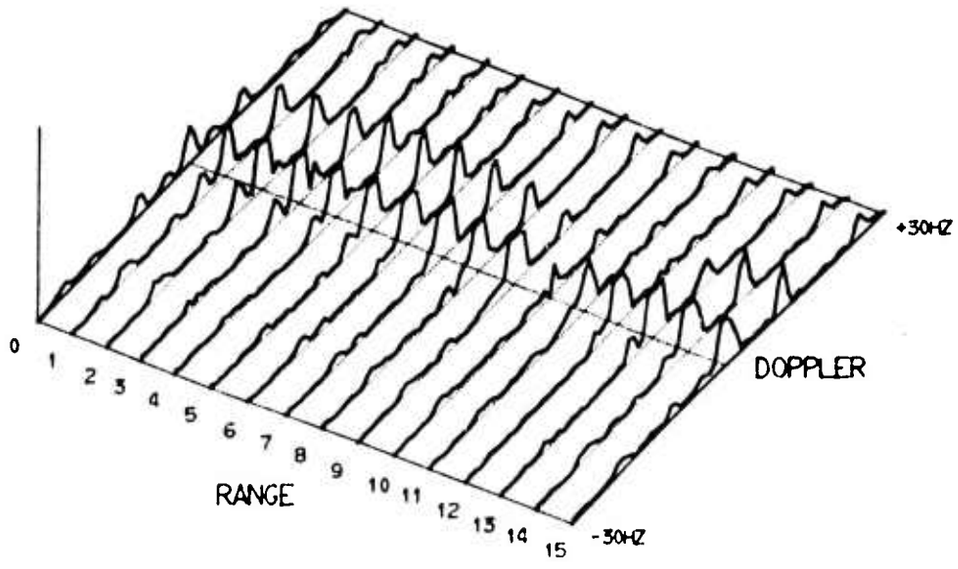

a) Frost algorithm

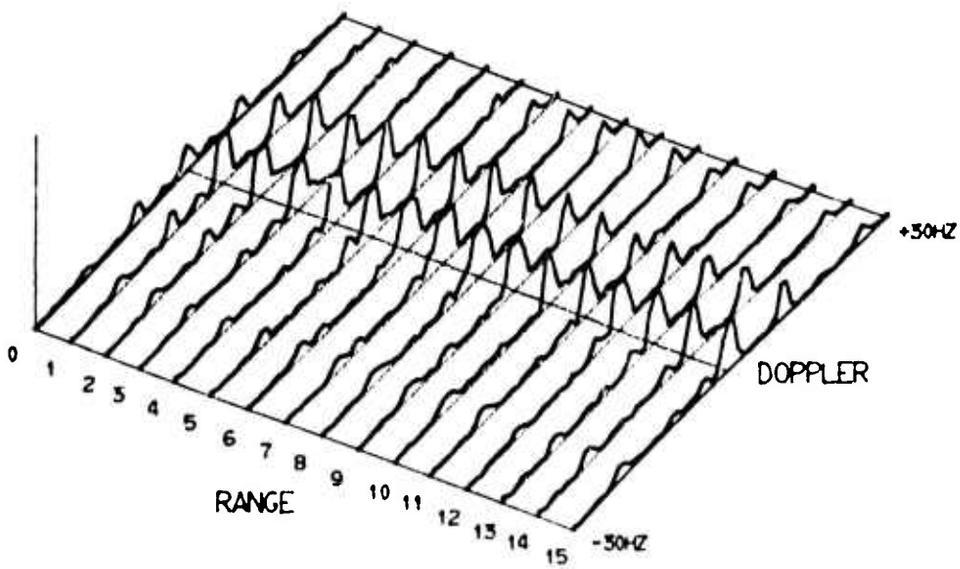

b) P-vector algorithm

Fig. 34. Constrained minimum mean-square error comparison for dwell no. 5, March 15, 1974

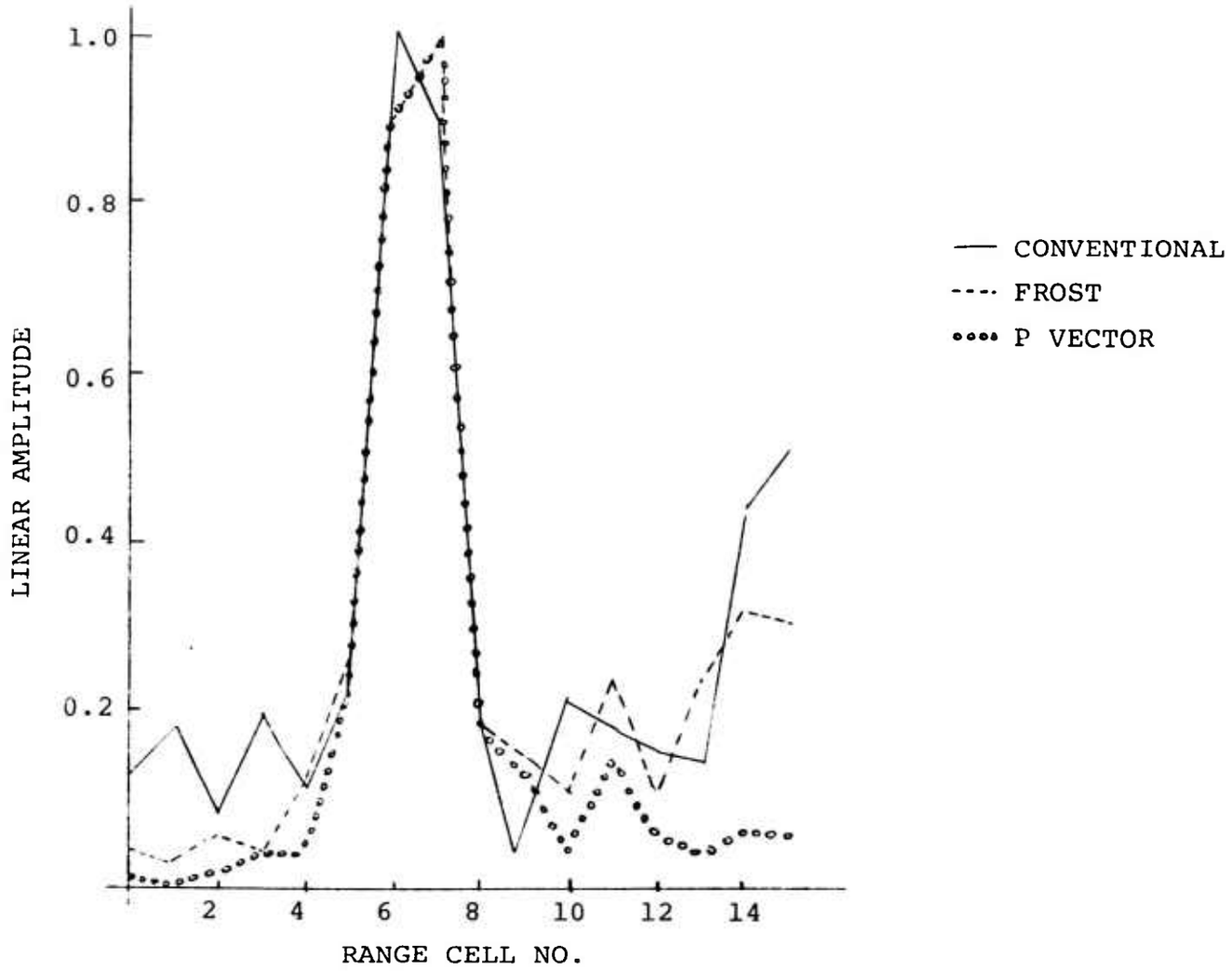

Fig. 35. Linear amplitude response observed in velocity cell -17 during dwell no. 3

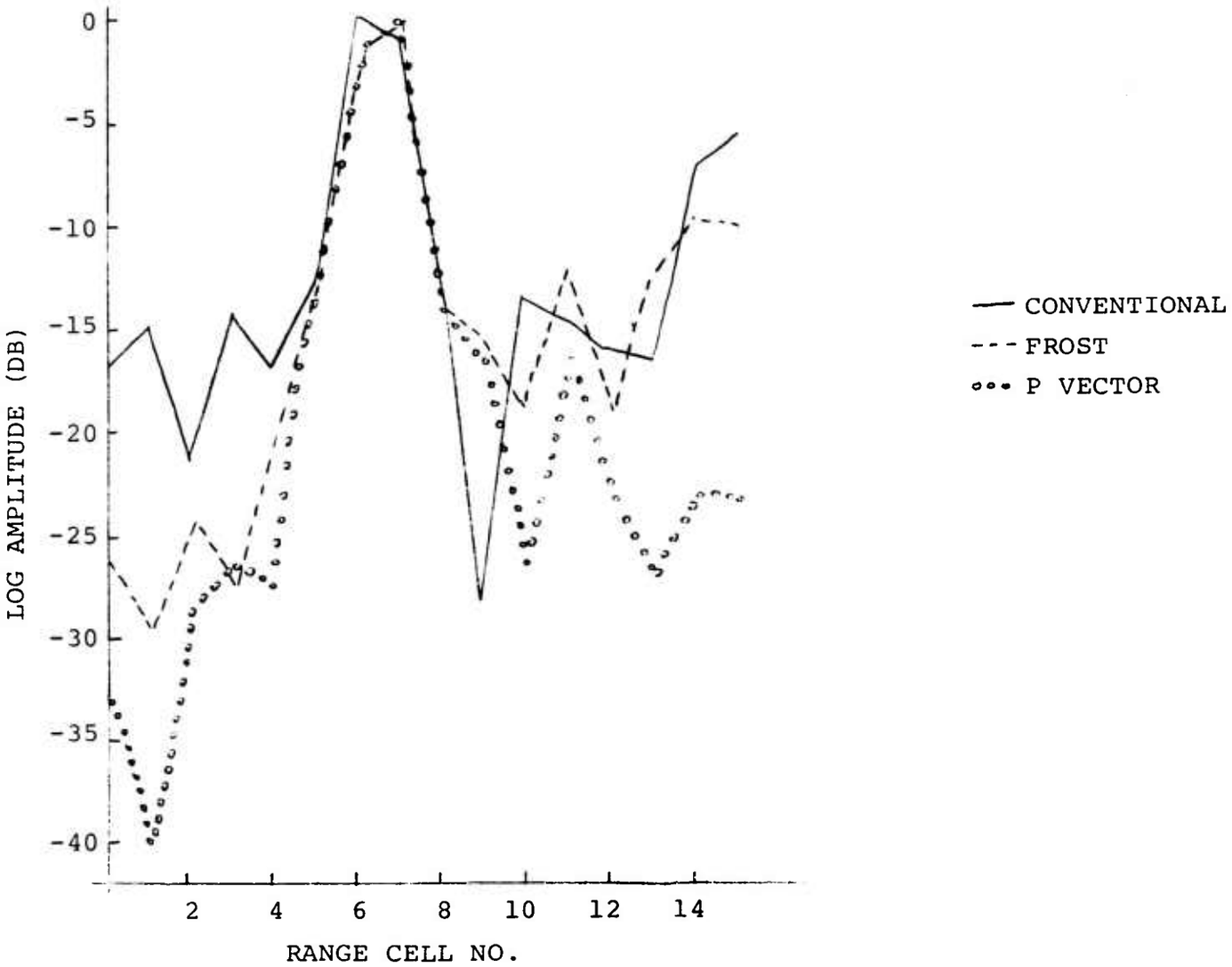

Fig. 36. Log amplitude response observed in velocity cell -17 during dwell no. 3

The frequency-independent nature of the boresight response of the Frost procedure is illustrated by the frequency/azimuth plot presented in Fig. 37. Comparison with the equivalent P-vector response given in Fig. 29 shows that the primary difference lies in the response observed at boresight (azimuth cell number 8).

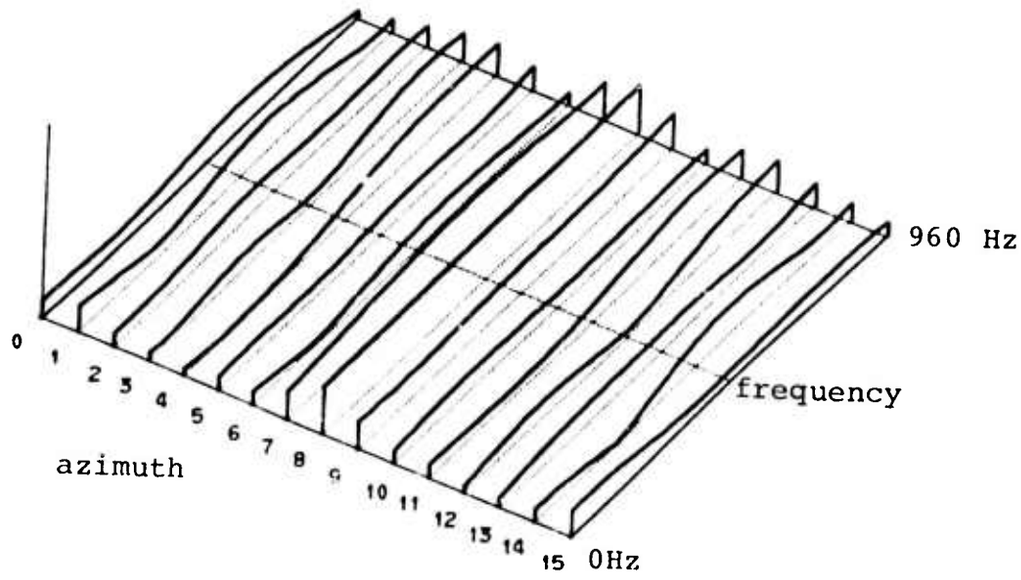

Fig. 37. Azimuth-frequency response for Frost adaptation algorithm at the end of dwell no. 3, March 15, 1974

VII. DISCUSSION AND CONCLUSIONS

This report has summarized the efforts carried out at the University of Colorado during the period March, 1974 to March, 1975 in support of the ARPA HF Adaptive Array Program. The emphasis at Colorado has been on the detailed analysis of adaptive beamforming characteristics, including the development and analysis of various algorithms, using a relatively small sample of field-recorded data. Detailed studies which test these procedures over longer time periods and under a variety of ionospheric and interference conditions need to be conducted for purposes of gathering a statistical history of adaptive beamforming performance. Fortunately, such studies have been conducted at SRI[4] during the past year using a real time implementation of the P-vector algorithm and will continue over the next year.

The results obtained at Colorado during the past year have substantiated earlier reported results.[2,3] Specifically, it has been demonstrated that substantial signal-to-noise and signal-to-interference improvements can be achieved in HF backscatter radar systems which employ time-domain adaptive beamforming methods. It has been shown that interference levels in the processed range/doppler maps can be reduced as much as 20 dB. In addition, the

overall noise floor, exclusive of those areas containing interference, is substantially lowered. Under every condition investigated to date, the adaptive beamformer has provided performance levels superior or equal to that offered by conventional processing. No conditions have been found in which the use of adaptive processing induced a degradation in performance.

Several new specific results were obtained during the course of the present study and have been grouped into four areas of investigation:

1. Coefficient Time-Variation Studies

It has been demonstrated that the time scale of the variation in optimal weights in an HF environment is the order of one second or less. In several cases, significant variability was noted within a time span as short as one half second. It was further demonstrated that the P-vector time-domain adaptation procedure can successfully track these variations when used with a step size value of $\alpha = 0.1$. The standard deviation of the adaptive weights about their time varying mean values was found to be the order of 2-3%. This is in excellent agreement with the value predicted by the theory of convergence of the adaptive algorithm for the case of stationary input statistics. Thus, although the signals observed at HF are non-stationary, the time scale of their variation is sufficiently slow so as to

be successfully followed by the P-vector algorithm. It should also be noted, however, that this conclusion holds only for a processor consisting of 40 adaptive weights. The theory of adaptive processing has shown that adaptive convergence times are approximately linearly related to the number of adaptive degrees of freedom in the system. Assuming that the time constant for the present system is about 0.1 second, this places an upper limit of about 200 coefficients for an adaptive signal processing system operating in an HF environment. At this level, the adaptive time constant would be about 0.5 seconds, a value insufficient to track the observed variations.

2. Clutter Suppression Studies

The use of individual clutter suppression filters at the individual subarray outputs has been investigated. For the rather small data sample used during this study (five successive one second dwells) it was found that MTI filters provided neither significant advantage nor significant disadvantage in processing. Signal-to-noise and signal-to-interference ratios measured in the range-doppler maps varied less than a few dB between using and not using three pulse clutter suppression filters. Cases were found where the use of MTI filters produced inferior performance and in other examples, superior performance over that obtained by adapting in the presence of clutter. Similar studies carried out by SRI[4] have indicated an example in which MTI

processing provided a seven dB advantage (see Fig. 12, Ref. 4). This advantage was observed only for a two second interval out of a nine second record, however, and for the remainder of the time, no significant advantage or disadvantage was evident.

It is difficult to draw definitive conclusions regarding the use of MTI filters in an adaptive beamforming system based upon the present evidence. Certainly, the qualitative argument which states that MTI filters must help due to the fact that the removal of clutter releases adaptive degrees of freedom is convincing. At this point, it appears that the use of clutter suppression devices is at yet unresolved and further investigative efforts in this area are warranted.

3. Aperture Tradeoff Studies

The effect of reduced aperture size on beamformer performance has been studied for both conventional and adaptive processing. A simple simulation model was used to demonstrate that in a non-isotropic noise environment, conventional processing does not provide increased output signal-to-noise plus interference ratio as elements are added to the array to expand the aperture. This model also demonstrates that adaptive beamforming in the same environment did provide a monotonically increasing performance with increased aperture size, but that a threshold aperture size existed above which the performance increase

was minimal.

Observations using experimental data confirmed that a reduction of up to one half the original aperture did not significantly reduce system performance when adaptive beamforming was in use. It was further found that the relationship between output SNR and aperture size for the case of two subarrays with variable spacing was not simply related to the aperture spanned by the subarrays. Specifically, processing subarray no's 1 and 4, which span one half of the available Los Banos aperture, produced larger target signals in the range-doppler display than did the processing of subarrays 1 and 8 (full aperture) or numbers 1 and 2 (one-eighth aperture). This result was observed for both conventional and adaptive beamforming methods. One possible explanation for these results is the prese-ce of a wave-like fading structure across the receiving array. Under such conditions, the question of optimal subarray spacing and location could be expected to change as the fading nulls move across the array. Further detailed investigations of this phenomena is warranted.

4. Minimum Mean-Square Error Adaptation with Constraints

A generalized time-domain adaptive procedure for minimizing the beamformed output power subject to a linear constraint on the processor coefficients has been implemented and tested using experimental data. Results have

shown that satisfactory convergence rates and performance can be achieved at a computational cost approximately 50% greater than that required for P-vector adaptation. The particular constraint studied in these tests provided a frequency independent response in the main lobe direction. It was shown that lower output signal-to-noise and signal-to-interference ratios are achieved with this method than with P-vector adaptation and that the difference may be as great as five dB in some range-doppler cells.

Suggestions for future work with constrained adaptive methods include:

a) Additional data processing to provide comparison with the P-vector method under differing ionospheric and interference conditions.

b) An investigation into the utility of linear constraints other than that of a frequency independent main lobe.

c) A study of the performance of the constrained procedures under conditions in which one or more hardware elements fail in the adaptive processor. It is conceivable that procedures designed to minimize output power may very well place a large weighting on a quiet but useless subarray output produced, for example, by failure of a preamplifier.

5. Suggestions for Future Studies

The following suggestions for future research in the area of adaptive beamforming at HF became evident during the course of the present investigations:

a) A study of additional time-domain adaptive procedures which are designed to optimize criteria other than minimum mean-square error should be conducted. This effort would include maximizing output SNR and the various methods of adaptive sidelobe cancelling which have been suggested. Comparisons with the existing least-squares techniques should be conducted using simultaneous processing of experimental data.

b) A detailed comparison between the time-domain, single receiver channel, tapped-delay-line method of processing discussed in this report and the alternative procedure of quadrature receiver processing should be carried out. Optimization in the latter case is generally achieved using correlation matrix estimation and inversion methods. Time-domain procedures for this class of receiver are also available, however, and should be included.

c) In most HF installations proposed to date, the number of receiving elements greatly exceeds the number of adaptive degrees of freedom which can be utilized. The problem of optimally distributing these degrees of freedom in the system--i.e. the

subarray geometry problem--is as yet unsolved and warrants further study. One reasonable approach to this rather ill-defined problem would be to consider only minimum redundancy and maximum redundancy configurations. The former case has been widely investigated by radio astronomers but has the distinct disadvantage that overall performance is greatly deteriorated by the loss of a single element, such as during a deep fading null. Maximal redundancy avoids this problem by distributing the degrees of freedom uniformly among the available elements.

d) Since any operational HF radar system will operate using multiple simultaneous received beams, further research must be conducted to determine the best hardware configuration for a multibeam adaptive processor. This study should include the possibility of performing separate FFT operations at each subarray output, prior to adaptation.

References

1. L. J. Griffiths, "Final Report: Adaptive antenna processing literature survey," Dept. of Electrical Engineering Report No. 13789, University of Colorado, Boulder, Colo., January, 1972.

2. L. J. Griffiths and M. Larimore, "Adaptive array processing of HF signals propagated over a 2600 km path," RADC-TR-73-75, (AD760137), Rome Air Development Center, Griffiss AFB, New York, January, 1973.

3. L. J. Griffiths, "Adaptive array processing of HF backscatter radar signals," RADC-TR-74-194, (AD783898), Rome Air Development Center, Griffiss AFB, New York, May 1974.

4. T. Washburn and L. E. Sweeney, Jr., "An on-line adaptive array processor for an HF backscatter radar," SRI-TR 28, Final Technical Report, Stanford Research Institute, Menlo Park, California, March, 1975.

5. O. L. Frost, III, "An algorithm for linearly-constrained adaptive array processing," Proc. IEEE, Vol. 60, No. 8, August, 1972.

6. B. Gold and C. M. Rader, Digital Processing of Signals, McGraw-Hill Co., New York, 1969.

7. A. Oppenheim and R. Schafer, Digital Signal Processing, Prentice-Hall Inc., New Jersey, 1975.

8. D. Lee and R. Compton, Jr., "Transient response of a power equalization array with coherent CW signals," QR-3234-2, Electroscience Laboratory, Ohio State University, Columbus, Ohio, March 1972.

9. L. E. Sweeney, Jr., "Spatial properties of ionospheric radio propagation as determined with half degree azimuthal resolution," SEL-TR-155, Stanford Electronics Laboratory, Stanford University, California, June, 1970.

10. L. J. Griffiths, "A simple adaptive algorithm for real-time processing in antenna arrays," Proc. IEEE, Vol. 57, No. 10, October 1969.

11. E. Kelley and M. Levin, "Signal parameter estimation for seismometer arrays," MIT-TR-339, MIT Lincoln Laboratory, Lincoln, Mass., January, 1964.

12. L. J. Griffiths, "A comparison of multidimensional Wiener and maximum-likelihood filters for antenna arrays," Proc. IEEE (letters), Vol. 55, No. 11, November, 1967.

13. A. Nuttall and D. Hyde, "A unified appraoch to optimum and suboptimum processing for arrays," USL-TR-992, U.S. Navy Underwater Sound Lab, New London, Conn., April, 1969.

MISSION
of
Rome Air Development Center

RADC is the principal AFSC organization charged with planning and executing the USAF exploratory and advanced development programs for information sciences, intelligence, command, control and communications technology, products and services oriented to the needs of the USAF. Primary RADC mission areas are communications, electromagnetic guidance and control, surveillance of ground and aerospace objects, intelligence data collection and handling, information system technology, and electronic reliability, maintainability and compatibility. RADC has mission responsibility as assigned by AFSC for demonstration and acquisition of selected subsystems and systems in the intelligence, mapping, charting, command, control and communications areas.